DESIGN AND APPLICATION OF CONFORMAL MAGNETIC AND GRAPHENE WAVEGUIDE ANTENNA

by

Abid Ahmad, B.S.

A thesis submitted to the Graduate College of
Texas State University in partial fulfillment
of the requirements for the degree of
Master of Science
with a Major in Engineering
August 2020

Committee Members:

Maggie Yihong Chen, Chair

Cecil Rich Compeau

Karl Stephan

FAIR USE AND AUTHOR'S PERMISSION STATEMENT

Fair Use

Duplication Permission

DEDICATION

I dedicate my thesis work to my family and many friends. A special feeling of gratitude to my loving parents.

ACKNOWLEDGEMENTS

I wish to thank my committee members Dr. Karl Stephan and Dr. Cecil R. Compeau who were more than generous with their expertise and precious time. A special thanks to Dr. Maggie Chen, my committee chair for her countless hours of reflecting, reading, encouraging, and most of all patience throughout the entire process.

I would like to acknowledge and thank to Dr. Andrew Foley and Dr. Leslie providing any assistance requested during my research. Special thanks goes to my research group for their continued support. I appreciate my friend, Keila, and Otto, for his encouragement throughout the whole process. At last, I would like to express my sincere gratitude all the people who have contributed their precious time to help me along the way.

TABLE OF CONTENTS

Page

LIST OF TABLES

Table **Page**

LIST OF FIGURES

Figure **Page**

ABSTRACT

This thesis investigates conformal magnetic and graphene waveguide antennas working at c-band for applications of wireless local area network (WLAN) and Wi-Fi networks. Antennas with magnetic material could be an extremely reliable and mature means for coupling and reshaping the incoming radiation pattern to increase the overall gain of the communication system. In this work, ferromagnetic paste and ink were developed, ferromagnetic thin film was deposited and characterized as DC and high frequency, in terms of conductivity, permittivity and permeability. The highest permittivity and permeability achieved are 12 and 29.5 respectively of strontium ferrite material. Then the measured data was used to design and simulate the ferromagnetic waveguide with High Frequency Structure Simulator (HFSS) software from ANSOFT. The simulation results of 25.4 cm × 17 cm × 0.0125 cm ferromagnetic antennas show improvement of signal gain of 1.1 dB over the source antenna. The graphene array antenna is also analyzed in order to show how the antenna changes the far field radiation pattern from a source since graphene's resistance to harsh environment is one of the approaches to solve the transportation communication challenge. The graphene antenna is tested to verify the simulation results. The array of magnetic/graphene antenna is proved to enhance the incoming signal from the patch antenna to propagate it along the magnetic/graphene antenna structure.

1. INTRODUCTION

Magnetic waveguide background

In communications engineering, the term waveguide indicates any linear structure that carries electromagnetic waves between its endpoints. In magnetic circuit design, closed magnetic loops have significantly greater circuit efficiencies than open circuits. For example, the ferrite loopstick is broadly used in AM-band antennas. Typically, the ferrite rod antennas operate using the ferrite material to concentrate the magnetic component of the radio waves through the pick-up coil. This is brought about by the high permeability μ of the ferrite. The magnetic antenna designs originate into the 1950s (Rumsey, V.,1958). In 2014, it was discovered that the magnetic antennas could be made into conformable and broadband antennas (Auckland, D.; Daniel, C et al., 2014). The recent development of ferrites having comparatively low loss and high permeability has opened the possibility of improving the performance of small loop antennas by the introduction of a ferrite core (T Simpson, 2007). The quality of magnetic material for loop antenna applications is determined by the ratio of the relative permeability to the relative permittivity (McLean, 2012). The concept of coupling the magnetic flux from one magnetic loop to another loop is also depending on the material properties and the geometry of the antenna.

Therefore, we have explored and developed the ferromagnetic material pastes and inks to create magnetic waveguide. At that point we have characterized all materials at DC (Direct Current) and high frequency around 5.9 GHz. From the characterization results, the material with higher permeability is chosen for antenna simulation and implementation. Finally, we simulated the antenna to evaluate the gain enhancement to a source antenna.

Prior work

The availability of waveguide antenna made of graphene or ferrite materials would greatly enhance the overall gain of the transmitter signal. This waveguide antenna would couple the signal coming from the transmitter to propagate along the prospective design of the waveguide antenna, which would directly lead to the much more rapid introduction of wireless local area network (WLAN) and Wi-Fi networks. This is especially true for transmitting signal for the long distance, which are less able to rely on pre-existing transmission/receiver infrastructure.

The ferrite antenna waveguide will be examined at 5.9 GHz to demonstrate the capability of c-band high frequency applications to cover the long distance communication. This distance can go down significantly on uneven topography which can lead to transmission loss; particularly, when using the omnidirectional transmission of the transmitter. Omnidirectional transmission of any source brings in losses proportional to one over the square of distance because of the signal going in all directions. However, we can minimize the transmission loss by directing the signal along the desired direction of the waveguide antenna structure. We investigate a group of novel ferrite inks with thermal and photonic sintering tools to create conformal waveguides, which can be applied to enhance the signal of transmitter having better directivity. This waveguide can economically broaden transmission length of c-band WLAN and Wi-Fi applications.

Problem statement

The problem is the attenuation of a signal from the source of transmitter. The goal of this research is to innovate peel and stick waveguide antenna which is capable of enhancing signal gain of transmitter or any source antenna by directing along the waveguide antenna structure. It can be split into the following tasks.

- Firstly, we researched what kind of material we are going to use and develop the ferromagnetic material paste and ink.
- The next step was to characterize all the material under both DC and high frequency
- Finally, simulated and tested the antenna to evaluate the enhancement to the gain from a source antenna.

Fig. 1.1 shows a diagram of a potential waveguide design, in which the magnetic circuits of ferrite loop antennae are closed by the adjacent antenna.

Figure 1.1: A diagram of a potential waveguide design of an array of antennae with loop circumferences roughly the wavelength of the signal (5.9 GHz corresponds to a free space wavelength of 2 inches)

Magnetic antennas couple into the magnetic component of the radio wave fields. Higher permeability allows efficient categorization of magnetic materials. (Auckland, D.; Daniel, C et al., 2014). The permeability of magnetic material is an important parameter. Based on other research work, we are choosing the material that has highest permeability among all the materials we evaluated. We have worked with a few different kinds of materials, and we found what strontium ferrite material would be best compared to barium and bismuth ferrite materials.

Moreover, we primarily built up the ferromagnetic ink which will have greater permeability since the material having greater permeability could be an amazingly reliable and mature method for foreseeing coupling and reshaping the approaching radiation pattern to build the overall gain of the communication system. After choosing the suitable material, we have characterized all the material at both DC and high frequency that have used in the simulation.

In high-frequency structure simulator (HFSS), the prospective antenna was designed. HFSS used to simulate the far-field radiation patterns and reshape the incoming radiation pattern. we designed a modest-sized magnetic antenna based on the best materials tested and the parameters from the simulation effort. The design simulation was mainly targeting at 5.9 GHz frequency since we are focusing on c-band applications.

In the simulation, a patch antenna radiating at 5.9 GHz is designed and verified using High Frequency Structure Simulator HFSS as it was considered as a source of radiation. The designed patch antenna is placed vertically in front of the prospective potential waveguide design to analyze the waveguide of the magnetic antenna. After that, we have optimized the structure of the magnetic waveguide by changing its position.

Since the antennas must be able to be printed/painted on a flexible substrate for peel and stick to a place, we have placed the magnetic waveguide on a dielectric substrate Kapton having relative permittivity 3.5 and relative permeability of 1. We have used a single antenna in order to enhance the overall gain of the patch antenna. Then, more antennas are added to repeat the same analysis to get the better directivity of the radiating element. We achieved better directivity along the desired direction instead of all direction, Therefore, this magnetic antenna having better directivity can be used for enhancing the incoming signal from the source of transmitting signal.

The importance to solve this problem would be very helpful for enhancing the incoming signal from the source of transmitting signal. Magnetic antenna having higher directivity is more cost effective instead of using active transmitters which would be expensive and challenging to implement along the magnetic antenna structure. Active transmitters also would require local power generation. Therefore, implementing magnetic antenna for the purpose of transmitting signal for the long distance would benefit to get rid of using more transmitter.

Material selection for the antenna

There are numerous books were written and countless papers published on magnetic materials each with its unique characteristics. The most basic classification of such materials based on its magnetic properties is quite literally done based on whether a material is magnetic or not in the presence or absence of an external magnetic field. Materials are broadly classified as being diamagnetic, paramagnetic, ferromagnetic, or anti-ferromagnetic. Among them, ferromagnetic materials are most useful for antenna applications as they have high permeability

(Sebastian, 2013). We have seen that some research identified few magnetic materials including nickel–zinc, iron oxide, and cobalt zirconium which exhibit a high relative permeability and low loss for designing the magnetic antenna on above the substrate in order to obtain high-performance at desired frequencies. (M. Rosales, 2001). Ferromagnetic film materials like it have the potential to attain much higher antenna efficiencies per unit weight than any ferromagnetic ceramic. Magnetic/nonmagnetic insulator multilayer films with thin magnetic layers can avoid eddy current losses, and are promising magnetic materials for use at high frequencies (Y. Kraftmakher).

Magnetic antennas having lots of advantage as it is a replacement to an electrical antenna. The proposed magnetic antenna will be very resistant to the harsh environmental conditions such as rain, snow, heat, surface friction. Moreover, magnetic antennas do not have as large of a drop in performance if the loop is broken because the magnetic field lines will continue to largely couple through the gap compared to an electrical antenna. Eventually, the magnetic antennas will be more cost-effective compared to the electrical one.

Research roadmap

We tried to provide a better understanding of the behavior of the magnetic ferrite material using DC analysis and high-frequency analysis. In DC analysis, measurements of the permeability, permittivity, and conductivity properties of thin films have been performed using a vibrating sample magnetometer (VSM), Hermes Probe, and Four-point probe station respectively. The samples examined using DC instrumentation were a baseline for this research. In the high-frequency analysis, measurements of the permeability, permittivity, and conductivity properties of thin films have been performed with a WR-137 waveguide. WR-137 (WR-137 is the size for a particular frequency ranges between 5.85 GHz and 8.2 GHz) waveguides are structures for guiding electromagnetic waves and are sometimes called a waveguide transmission line. From the results obtained, strontium ferrite materials provide the best performance compared to bismuth and barium ferrite materials in both the DC analysis and high-frequency analysis.

To give a clear insight into this research, the following list of chapters describe how research roadmap can be assessed and evaluated.

Chapter 1: The problem statement and its importance and how we are going to solve the problem are clearly explained in this chapter.

Chapter 2: Chapter two discusses materials development and its characterization procedure under the DC and high-frequency investigation.

Chapter 3: Chapter three discusses the graphene antenna simulation, fabrication, testing, and compared the results.

Chapter 4: Chapter four discusses the magnetic antenna simulation, and results.

Chapter 5: Chapter five covers the conclusion and future work.

2. CHARACTERIZATION OF MAGNETIC MATERIALS UNDER DC AND HIGH FREQUENCY

Introduction

The chapter is mainly focused on finding the permittivity, permeability and conductivity of several ferrite films using DC analysis and high frequency analysis. Permittivity stands for the resistance to the formation of electric field within a substance. Permeability represents the ability to sustain a magnetic field. Their real parts represent the energy storage ability, while imaginary parts are related to the dissipation of energy. DC characterization of ferrite films were considered as a benchmark research. At high frequency, it is important to know the characteristics of ferrite materials as the magnetic properties of materials are very important, and it helps to understand the fundamental structure and behavior of many materials.

Material development and ink characterization

In this thesis, several Ferrite samples placed on Kapton substrate were prepared in order to analyze its characteristic in waveguide method as well as for DC measurements. Ferrite materials, e.g. spinels and garnets, have attracted a lot of research interest in recent times because of their excellent microwave frequency characteristics such as low magnetic loss. Bulk ferrite materials have been widely used in the manufacture of microwave devices such as modulators, circulators, etc (J. Chen, 1995). However, thin films of ferrite materials have unusual electrical, mechanical, and optical properties compared to their bulk counterparts. Therefore, desirable magnetic properties of ferrites can be engineered at the sub-micron level and are easy to control. For example, the magnetic properties of Zinc-ferrites thin film have been reported to show a sharp deviation from the bulk (L. Chao, 2012). Furthermore, the permeability of 0.6 μm Nickel-Zinc ferrite thin film deposited on a 2 mm glass substrate by spin-spray exhibits a higher permeability than the Snoek's limit of bulk Ni-Zn (I. Youngs, 2005). Ferrite magneto dielectric materials are promising for antenna miniaturization and enhanced performance at microwave frequencies (A. Bahadoor, 2005). In this research, we chose Ni-Zn ferrite, Mn ferrite materials for ink formulation for high permeability design components.

Hexaferrites such as Sr- and Ba-doped hexaferrites together with bismuth ferrite (BFO), have many properties, which make them suitable for the magnetic waveguide (A. Kumar, 2008; D.S Mathew, 2007). We focused ink development on Ni-Zn, Mn, Sr, Bi and Ba ferrites. The hexaferrite materials having higher permeability can be used for the magnetic waveguide design in the radio frequency band of interest (i.e. c-band).

DC characterization

We have characterized the ferrite materials in DC condition. DC measurement provides analysis for the intrinsic and static properties. The AC measurement offers analysis for the behavior of the materials under dynamic conditions. We have utilized the DC estimation as the gauge to proceed onward AC estimation.

XRD analysis

X-ray diffraction (XRD) is a technique used in materials science for determining the atomic and molecular structure of a material. X-ray diffractometers consist of three basic elements: An X-ray tube, a sample holder, and an X-ray detector. An incident X-rays is generated from the X-ray tube and the intensities and scattering angles of the X-rays that are scattered by the material is picked up by an X-ray detector. The intensity of the scattered X-rays is plotted as a function of the scattering angle, and the structure of the material is determined from the analysis of the location, in angle, and the intensities of scattered intensity peaks. (Katsuhiko Inaba,2013)

Rigaku SmartLab X-ray Diffractometer (XRD) is used to analysis on the photo sintered strontium ferrite (FeSr) cured with the increasing voltage shown in Fig. 2.1. The effect of increasing the voltage is to increase the overall energy delivered to the sample.

The XRD Fig. 2.1, shows that the peaks become more intense and narrow as the voltage increases which is an indication of an increase in crystal domain size.

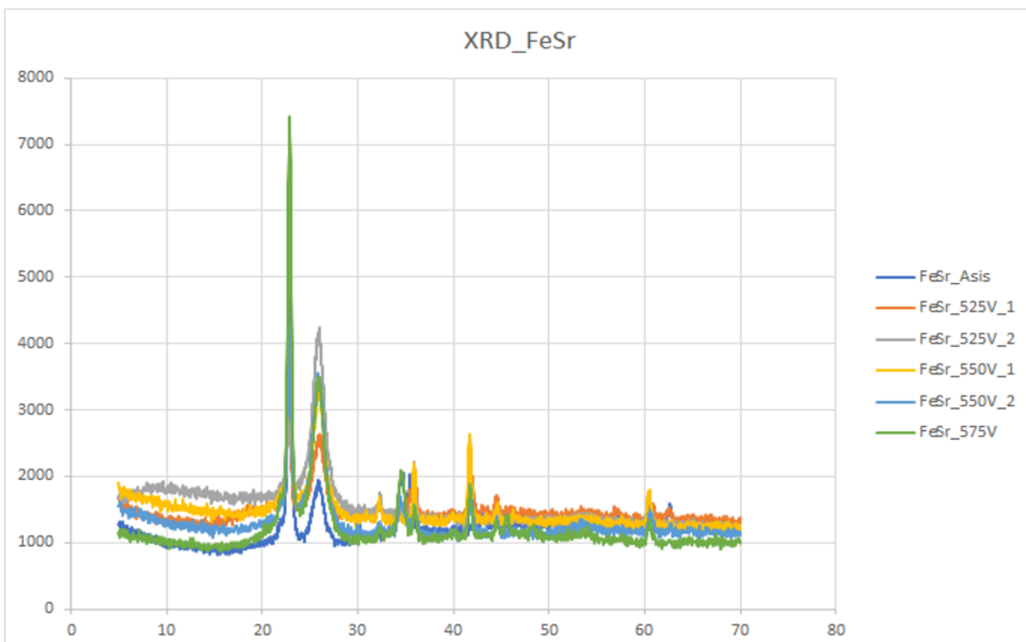

Figure 2.1: XRD analysis of as made and photosintered strontium ferrite

The XRD pattern of the printed Mn-ferrite thin film in Fig. 2.2, shows peaks corresponding to only single-phase particles, as well as a uniform spinel structure.

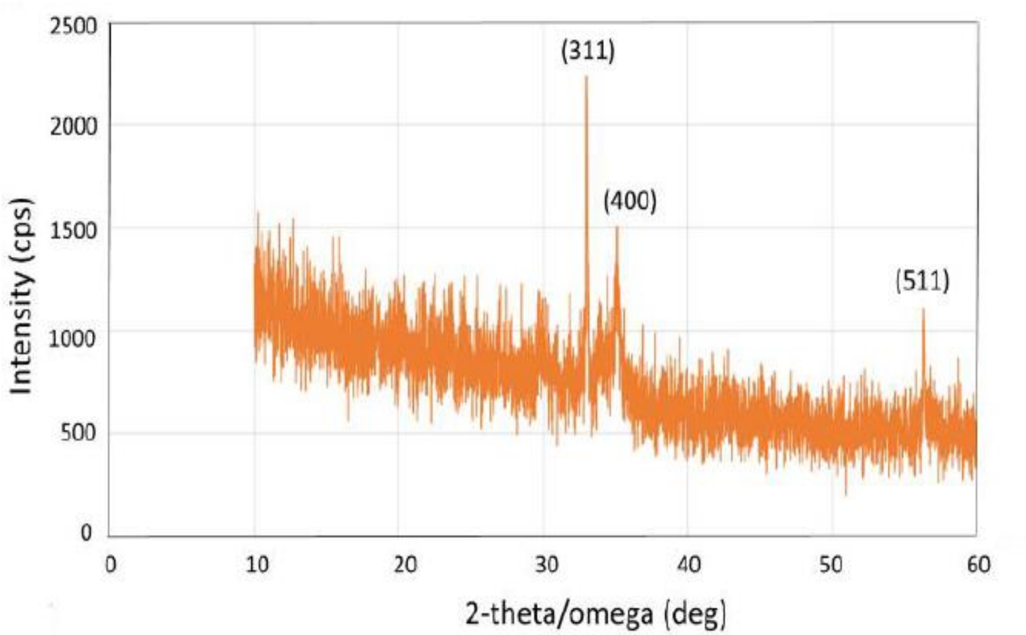

Figure 2.2: XRD measurement of Mn-ferrite thin film

The average crystallite of the thin film was calculated to be 31 nm using the full width at half-maximum (FWHM) of the diffraction point based on the Scherrer's formula. Scherrer's formula can be written as

$$L = \frac{0.9\,\lambda}{\beta\ \mathrm{Cos}\theta} \tag{2.1}$$

where L is the grain size, β is the full width at half maxima (FWHM), λ is the wavelength of the X-ray used, and θ is the Bragg's angle.

VSM analysis

A vibrating sample magnetometer (VSM) is used to measure the permeability behavior of magnetic ferrite materials. It operates on Faraday's Law of Induction, which conveys us that a changing magnetic field will yield an electric field potential.

The samples having 7 mm length, 6 mm width, 1.5 micron thickness was mounted on the 8mm Transverse Rod. Applied field was given from -2.1 T to 2.1 T with 400 sweep rate. As the sample is moved up and down, this magnetic stray field is changing as a function of time and can be sensed by a set of pick-up coils. The alternating magnetic field will cause an electric field in the pick-up coils according to Faraday's Law of Induction**.** This current will be proportional to the magnetization of the sample. The measured magnetic moment in e.m.u. units vs applied field is given below.

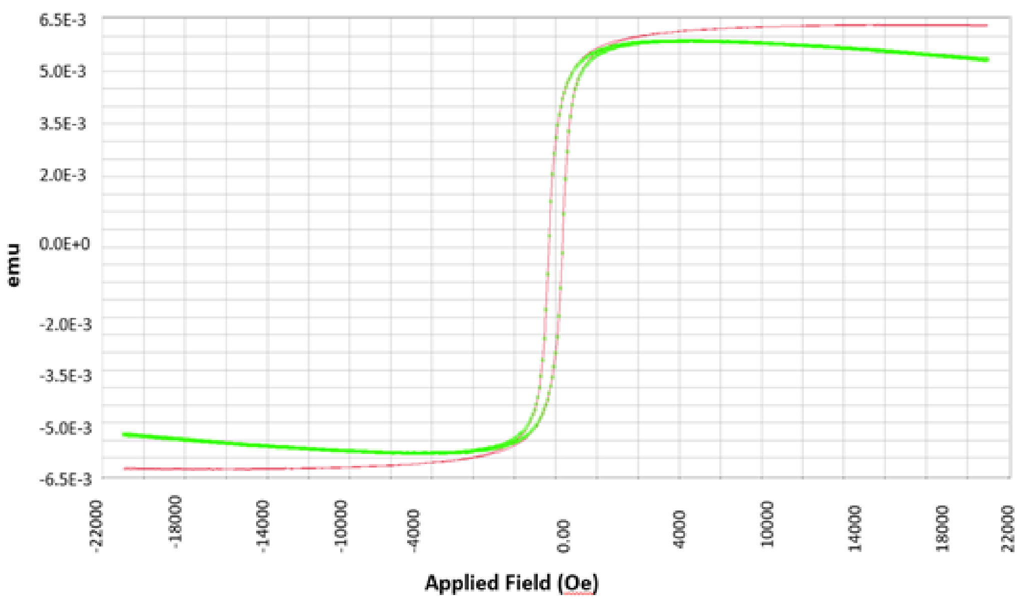

Figure 2.3: Magnetization (emu) vs. applied field (Oe)

The absolute permeability of FeoSr Sample is calculated 4.547*10^-6 Henries per meter (H/m) using VSM, and the relative permeability can be calculated using bellow equation

$$\frac{\text{Absolute permeability of the FeoSr}}{\text{Permeability of Air}}$$

Where the Permeability of air is 1.25663753*10^-6 (H/m), Thus, the relative permeability is 3.6183.

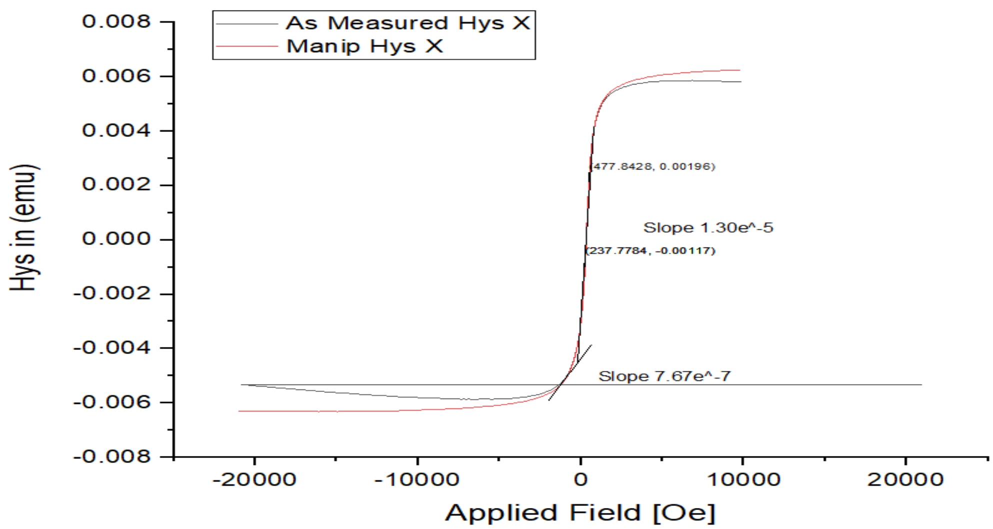

Figure 2.4: Slope calculation from the Hysteresis graph

Using Origin Software, slope was calculated 1.30e^-5, thus the relative permeability is 10.34. A summary of the results for the Ferrite films in table form is given below

Table 2.1: Obtained relative permeability from Origin

Materials	Relative Permeability measured in Origin
Strontium Ferrite	10.34
Bismuth Ferrite	12.57

We have obtained the Hysteresis loop by using a vibrating sample magnetometer. To get the maximum permeability of the sample, we have calculated the slope where the sample has better magnetization. From the Origin software, we calculated the highest slope in hysteresis loop which provides the more accurate value of permeability for a particular sample.

Probe station hermes analysis

Probe station Hermes is a specialized sample stage for probing thin film reactance (C, L, R) without a top contact. Liquid Mercury is applied via vacuum to a surface of the specimen and the back of the specimen is used as the other electrical contact. The samples on Silicon wafer were analyzed in order to measures to permittivity at 0-100 kHz using Hg probe.

In order to calculate the absolute permittivity, $\epsilon = \frac{C*d}{A}$ equation is used where the thickness of sample is $d = 7.5 * 10^{-6}$ m and area is $A = 4.72888 * 10^{-7} m^2$, And the relative permittivity is $\epsilon_r = \frac{\epsilon}{\epsilon_0}$ where $\epsilon_0 = 8.85 * 10^{-12}$ m farad per meter (F/m). The ferrite samples were examined to find the capacitance at a fixed AC 100 kHz while DC Bias has been varied from -1 to 1 and -5 to 5.

A summary of the results for the Ferrite films in table form is given below.

Table 2.2: Obtained relative permittivity of materials at (1-100) kHz

Materials	Relative Permittivity at 1kHz	Relative Permittivity at 100kHz
Barium Ferrite	17.5	19
Bismuth Ferrite	517.3	407.9
Strontium Ferrite	6.48	6.9

These higher values are reasonable when considering that BFO is a ferroelectric material.

Conductivity measurements

Resistivity is a fundamental characteristic of electrical materials and the measurement accomplished using a Source Measurement Unit (SMU). Sheet resistance/resistivity is the resistance of a square of the conductive thin film with uniform thickness. The sheet resistance is measured using the Van Der Pauw technique. We have cut the sample as a square shape and applied voltage on the sample with four contact pads. The resistivity of the as made and photo sintered films were measured. The results are tabulated below.

Table 2.3. DC resistance parameters for different ferrite films

Sample	Sheet Resistance (Kohm)	Resistivity (Kohm*μm)
Strontium Ferrite as Made	44.26	88.5
Strontium Ferrite as Photo sintered	0.05	0.11
Barium Ferrite as Made	41.3	331
Barium Ferrite as Photo sintered	1.6	12.8
Bismuth Ferrite as Made	31.7	190
Bismuth Ferrite as Photo sintered	16.5	99.2

AC characterization

In AC Characterization, we have characterized the magnetic thin-film to demonstrate their suitability for using in potential waveguide design of an array of antennae since it is important to know the magnetic properties of suitable materials. The permeability is the most important parameter to define, because it governs the interaction between the electromagnetic wave and the material, and is thus the origin of all magnetic phenomenon. Our work consists of performing the characterization of thin films at frequency of 5.9 GHz.

Basic principle

Many methods are available to characterize thin films at microwave frequencies. An older and simpler approach is to insert a sheet of the film to be measured into a rectangular waveguide that covers the frequency range of interest. A segment of a rectangular waveguide where a sample has been placed, filling the line and leaving no air gaps is a typical measurement configuration.

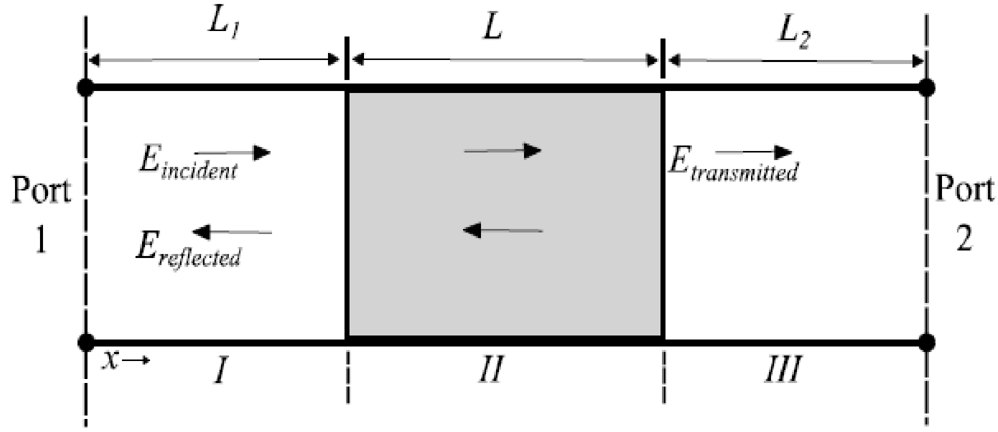

Figure 2.5: Incident, transmitted and reflected electromagnetic waves in a filled transmission line

Above figure is shown such a segment whose axis is in x-direction same with the propagation direction. The electric fields at the three sections of the transmission line are $E_{\mathrm{I}}, E_{\mathrm{II}}$ and E_{III}, respectively. The total length of the transmission line can be expressed as L_{Total}=L+L_1+L_2

We have measured the S parameter of the magnetic materials using a vector network analyzer. S-parameters describe the input-output relationship between ports (or terminals) in an electrical system. For instance, if we have 2 ports, then S_{12} represents the power transferred from Port 2 to Port 1. S_{21} represents the power transferred from Port 1 to Port 2 (Chen, 2004).

Experimental setup

Measurements of the microwave properties of thin films have been performed with a waveguide technique. The samples examined were a kapton film, a kapton film with bismuth ferrite ink or sintered coating on it, a kapton film with strontium ferrite ink or sintered coating on it. Samples of these films were cut into a size suitable for insertion into a WR-137 waveguide shown in Figure 5 and covered the entire waveguide cavity with the film. It was calibrated by normalizing to an air-filled cavity. Two independent scattering parameters S_{11} (essentially, the reflection coefficient at port 1 when port 2 is matched) and S_{21} (the transmission coefficient from port 1 to port 2) data measured with an Keysight N9917A vector network analyzer at 70 to 140 frequency steps from 5.85 to 7.8 GHz.

The parameters measured by the vector net-work analyzer were used to derive the real and imaginary parts of permittivity and permeability of the sample. The accuracy of the constitutive material properties depends on the accuracy with which the-parameters are measured. Since the experimental set-up involves several components such as cables and connectors, proper care has to be taken to ensure that the entire system remains stable over the measurement period. Measurement process might be compensated only for phase shift and losses in the empty-waveguide setup, errors due to reflections from the waveguide-to-coax transition. These errors were reflected and evaluated in the measured parameters of the commercial Kapton substrate. We have used Origin software to smooth the data. The Gaussian fit was used to the calculated permeability and permittivity data, which will be shown along with the non-smoothed data in the following graphs.

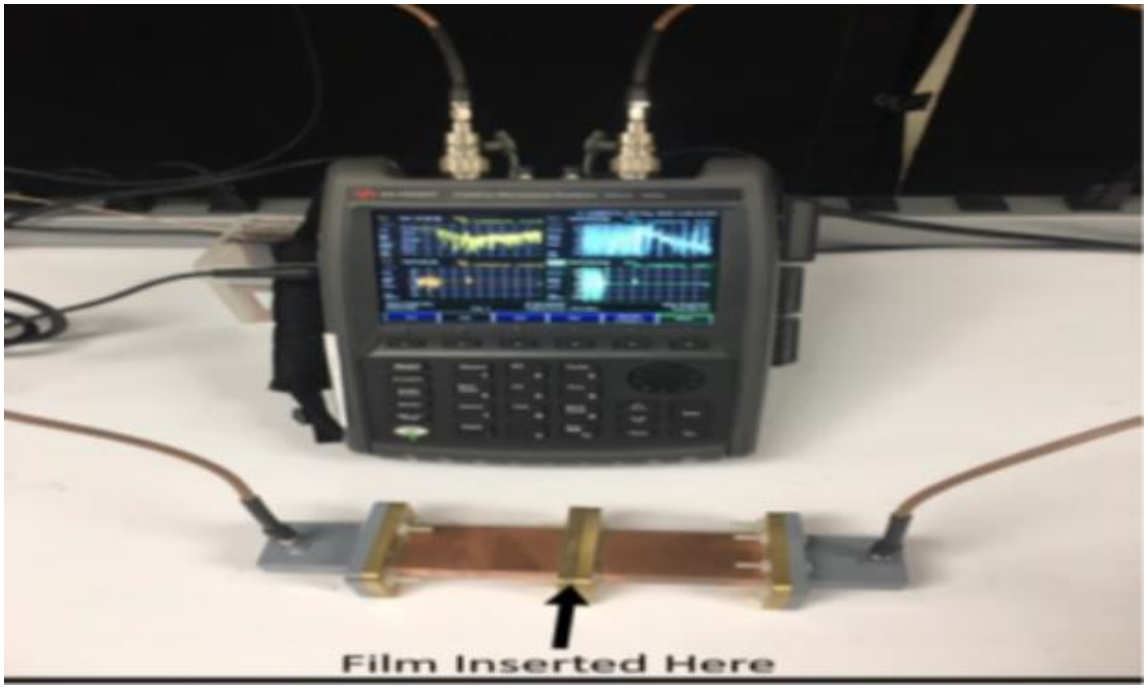

Figure 2.6: The waveguide setup for measuring AC permeability and permittivity.

(Top) VNA (Bottom) waveguide.

Nicolson-Ross-Weir (NRW) algorithm

Nicolson-Ross-Weir (NRW) algorithm is used in order to calculate the permeability and permittivity of the ferrite Film. The electric and magnetic behavior of a low-conductivity material is determined by two complex parameters, permittivity ε and permeability μ.

$$\varepsilon = \epsilon' - j\varepsilon'' \tag{2.2}$$

$$\mu = \mu' - j\mu' \tag{2.3}$$

Permittivity describes the interaction of a material with the electric field applied on it and respectively permeability describes the interaction of a material with the magnetic field applied on it. In microwave electronics are often used the relative permittivity ε_r and relative permeability μ_r, where ε_0 and μ_0 are the permittivity and permeability of the free space.

$$\varepsilon_r = \frac{\varepsilon}{\varepsilon_0} = \varepsilon_r{}' - j\varepsilon_r{}'' \tag{2.4}$$

$$\mu_r = \frac{\mu}{\mu_0} = \mu_r{}' - j\mu_r{}'' \tag{2.5}$$

The Nicolson-Ross-Weir (NRW) algorithm combines and derives formulas for the calculation of permittivity and permeability.

$$\gamma = X \pm \sqrt{X^2 - 1} \tag{2.6}$$

$$X = \frac{\left(S_{11}{}^2 - S_{21}{}^2\right) + 1}{2S_{11}} \tag{2.7}$$

Where γ is a complex number which is used to describe the behavior of an electromagnetic wave along a transmission line. The appropriate sign is chosen so that $\gamma \leq 1$ in order to express the passivity of the sample. The transmission coefficient is

$$T = \frac{(S_{11} + S_{21}) - \gamma}{1 - (S_{11} + S_{21}) * \gamma} \tag{2.8}$$

The complex permeability is calculated from

$$\mu_r = \frac{1 + \gamma}{(1 - \gamma) * \Delta * \sqrt{\frac{1}{\lambda_0{}^2} - \frac{1}{\lambda_C{}^2}}} \tag{2.9}$$

and the complex permittivity from

$$\varepsilon_r \mu_r = \lambda_0{}^2 \left(\frac{1}{\Delta^2} + \frac{1}{\lambda_C{}^2}\right) \tag{2.10}$$

With

$$\frac{1}{\Delta^2} = -[\frac{1}{2\pi D}\ln(\frac{1}{T})]^2 \quad (2.11)$$

Where λ_C is the cutoff wavelength of the transmission line section, λ_0 the free space wavelength and $\frac{1}{\Delta} = \frac{1}{\lambda_g}$ where λ_g is the transmission line guide wavelength. (Alexandre, Vicente, 2011).

The equation 2.11 has an infinite number of roots since the imaginary part of the logarithm of a complex quantity T is equal to the angle of the complex value plus $2\pi n$, where n is equal to the integer of $\frac{L}{\lambda_g}$. This condition is equivocal in light of the fact that the period of the transmission coefficient T doesn't change when the length of the material is expanded by a different of frequency.

The unwrapping method can be used to solve the problem of phase ambiguity. Determination of the initial phase is needed and then phase unwrapping. For a sample with constant permittivity over a wide frequency range, the phase of T fluctuates between $\pm\pi$. Phase ambiguity arises from the phase wrapping effect. Equivalent to phase unwrapping is to obtain the correct additive constant of $2\pi n$ (Chen, 2004).

A straightforward and normal approach to unwrap the phase is by identifying a hop in phase value of more than π from one measurement frequency to the next and then shifting all the subsequent phases by 2π in the opposite direction.

Results

<u>Kapton Film</u>

Since all of the ferromagnetic films were deposited on the Kapton film, the Kapton film was characterized first. The permeability of Kapton film is measured by finding its reflection data (S) using the waveguide at 5.9 GHz frequency. The phase resolution of the S parameter is good enough to provide fairly accurate data on finding the sheet permeability, permittivity and conductivity. The relative permeability is measured to be 1.33 at 5.9 GHz, which gives us 33% accuracy. The error comes from the calibration error of equipment and the air gap between the waveguides.

Since Kapton has a small relative permeability compared to the magnetic films, we can ignore its effect while we process the data of the magnetic films.

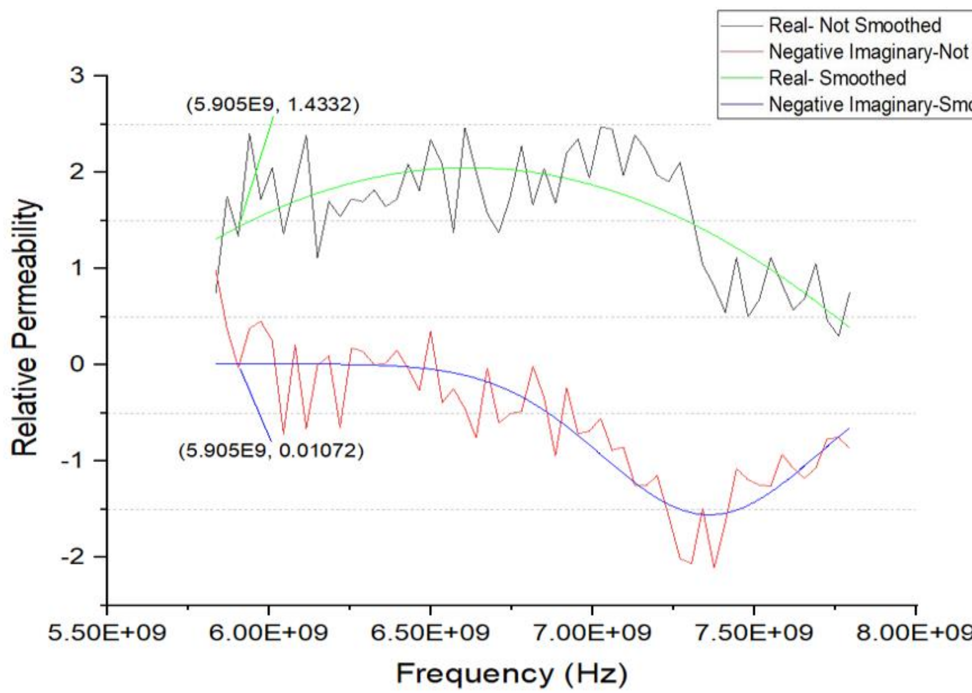

Figure 2.7: Relative permeability of Kapton film

. In Fig. 2.7 and Fig. 2.8, unprocessed permeability, permittivity data ("Not smoothed") and the Gaussian fits permeability, permittivity data ("smoothed”) at 5.9 GHz are shown.

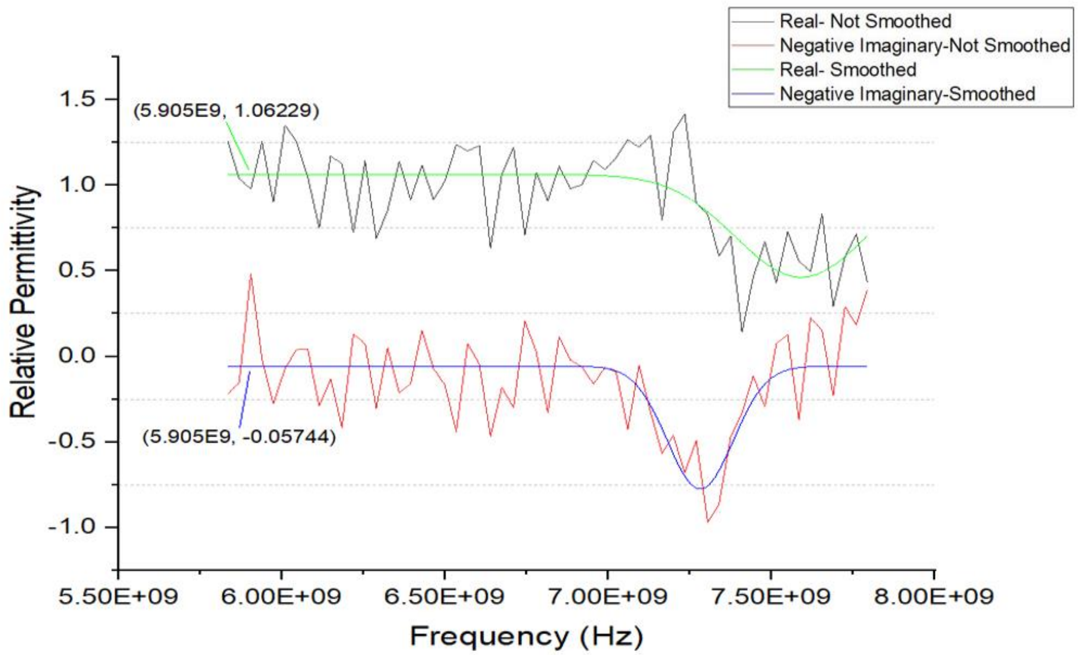

Figure 2.8: Relative permittivity of Kapton film

Fig. 2.8, shows averaging real part and imaginary part of the permittivity of the kapton film are 1.06229 and -0.05744 respectively at 5.9 GHz frequency

The ferrite samples results are given below.

Bismuth-ferrite_film

In Fig 2.9, Bismuth ferrite also exhibited that it has a higher permeability about 8.76 average at high frequency.

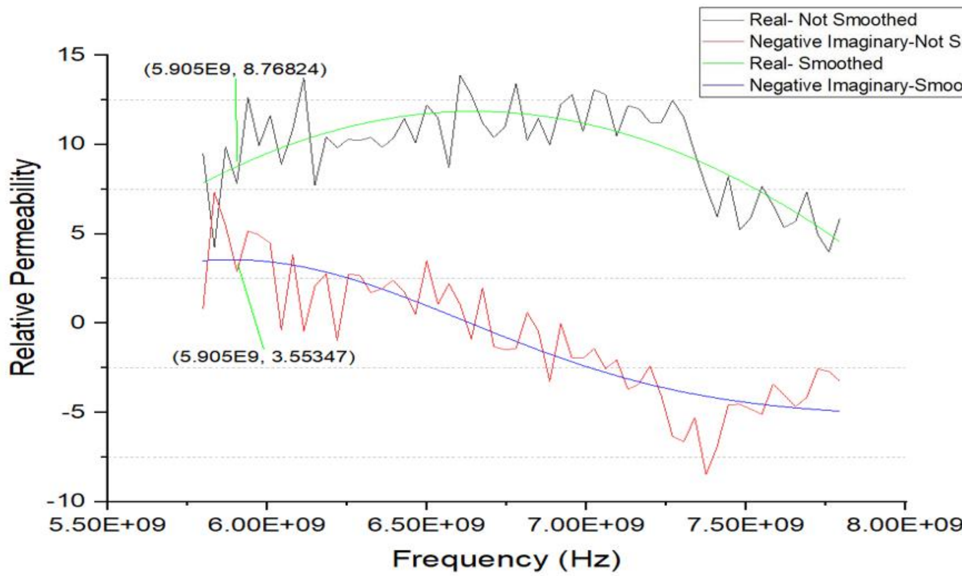

Figure 2.9: Relative permeability of Bismuth-ferrite film

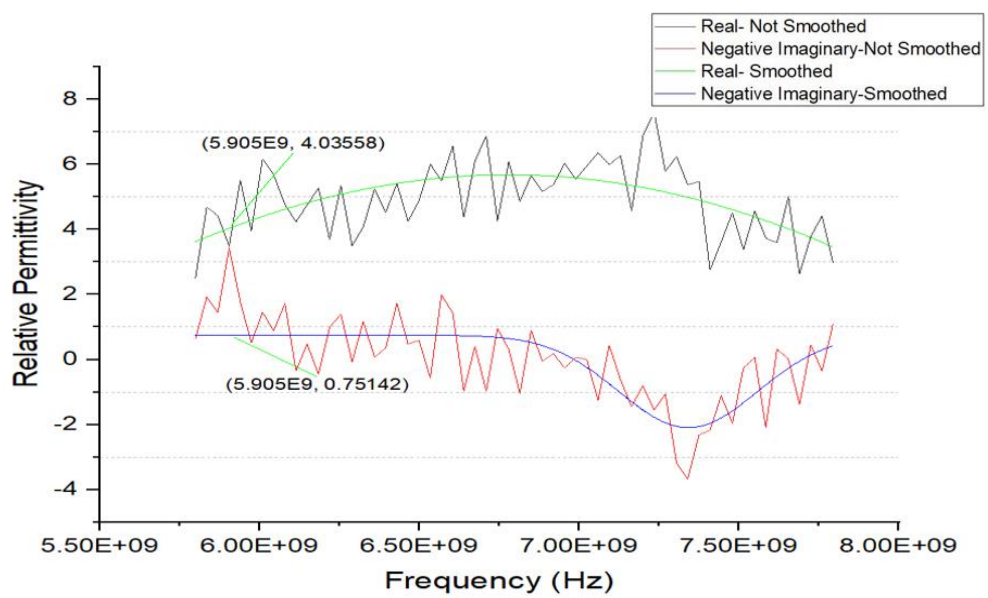

Figure 2.10: Relative permittivity of Bismuth-ferrite film

Bismuth-ferrite sintered film

The permeability of bismuth ferrite sintered film was found to increase and demonstrated that it has good magnetic properties. In Fig 2.11, Bismuth ferrite sintered film shown that it has almost permeability about 15.05 average at high frequency.

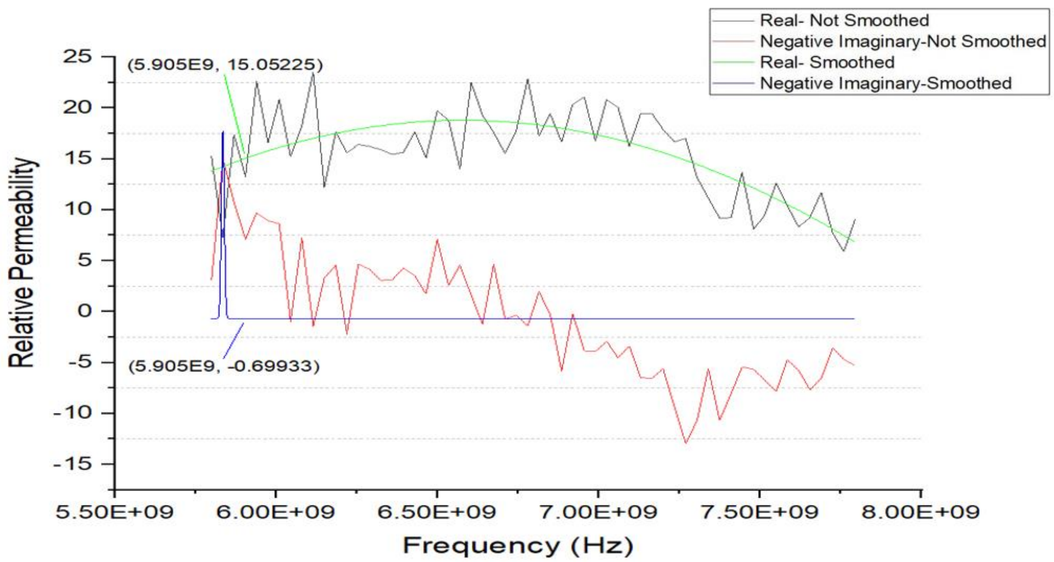

Figure 2.11: Relative permeability of Bismuth-ferrite sintered film

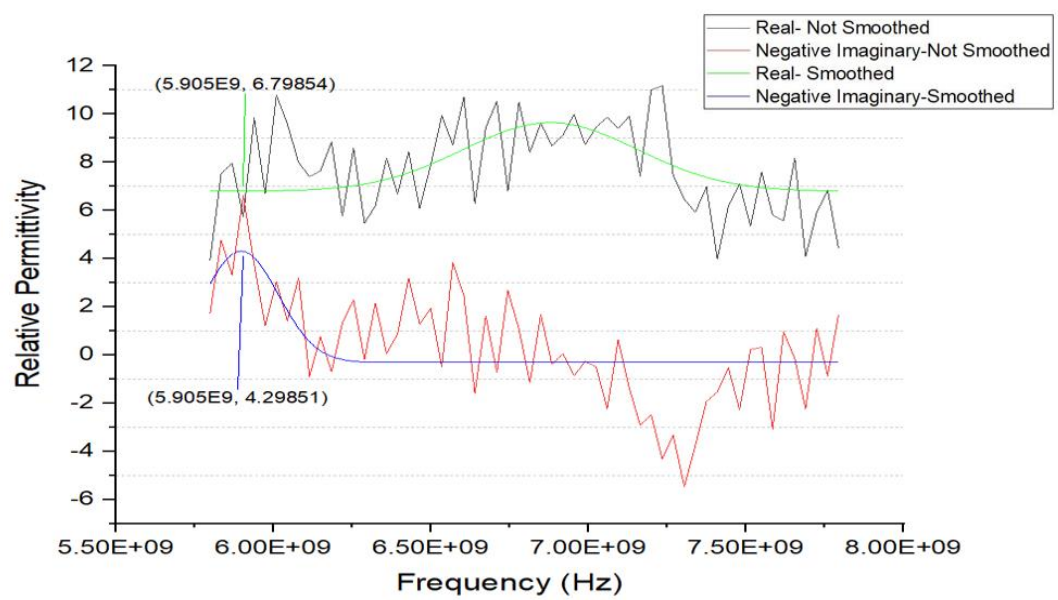

Figure 2.12: Relative permittivity of Bismuth-ferrite sintered film

Strontium-ferrite_film

Strontium Ferrite film showed that real permeability of 11.41 and real permittivity of 4.90 which was useful for this film.

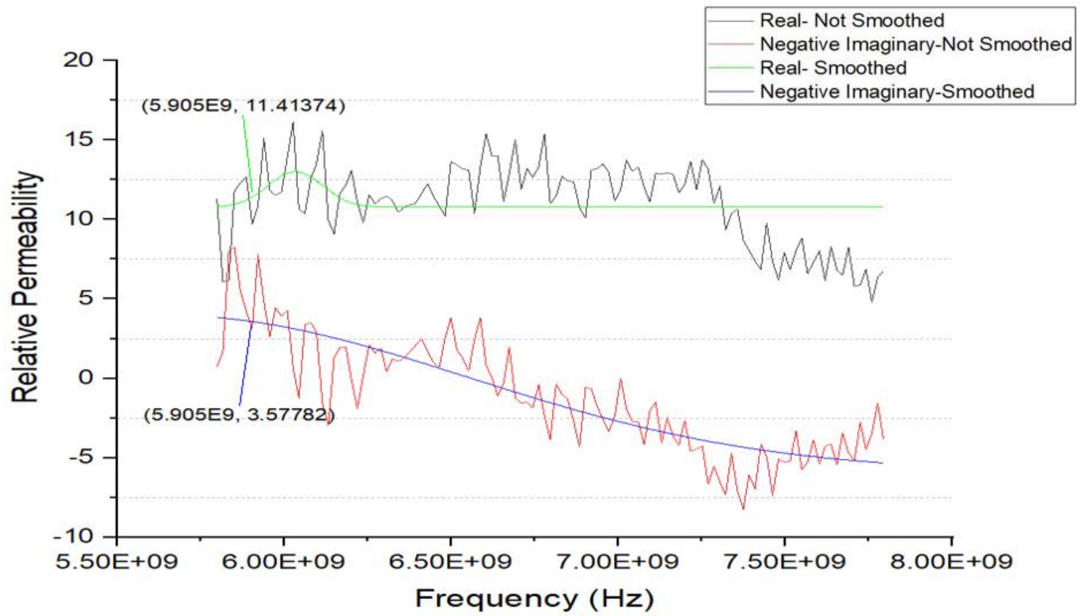

Figure 2.13: Relative permeability of Strontium-ferrite film

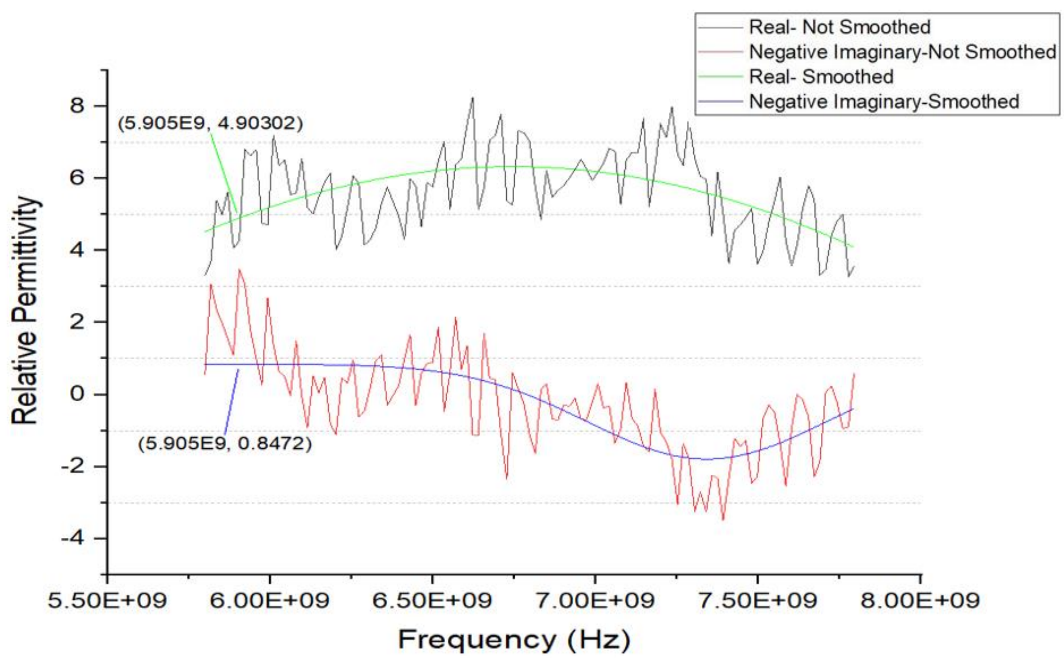

Figure 2.14: Relative permittivity of Strontium-ferrite film.

Strontium -ferrite sintered film

The Strontium Ferrite sintered film is seen as best example since it gives higher relative permeability about 29.51. The reflection from the film was huge enough with the goal that exact information was realistic from both S_{11} and S_{21} informational indexes. The obtained S parameter values are used to find the relative permeability and relative permittivity of the Strontium ferrite sintered film. From the outcomes, we can conclude that the Strontium Ferrite sintered film has a real and imaginary relative permeability with an estimation of 29.51 and 1.80 separately which is higher than the barium ferrite and bismuth ferrite.

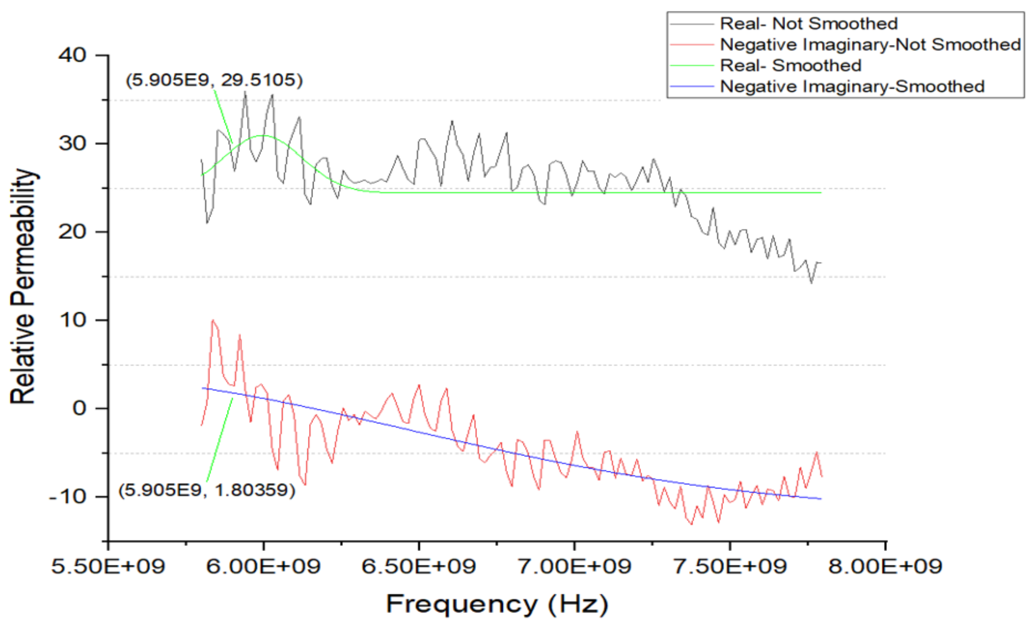

Figure 2.15: Relative permeability of Strontium-ferrite sintered film

Fig. 2.16 shows that Strontium ferrite film has a real and imaginary relative permittivity with a value of 12.86 and 0.3154 respectively which is higher for the Strontium ferrite sintered film than other measured sample.

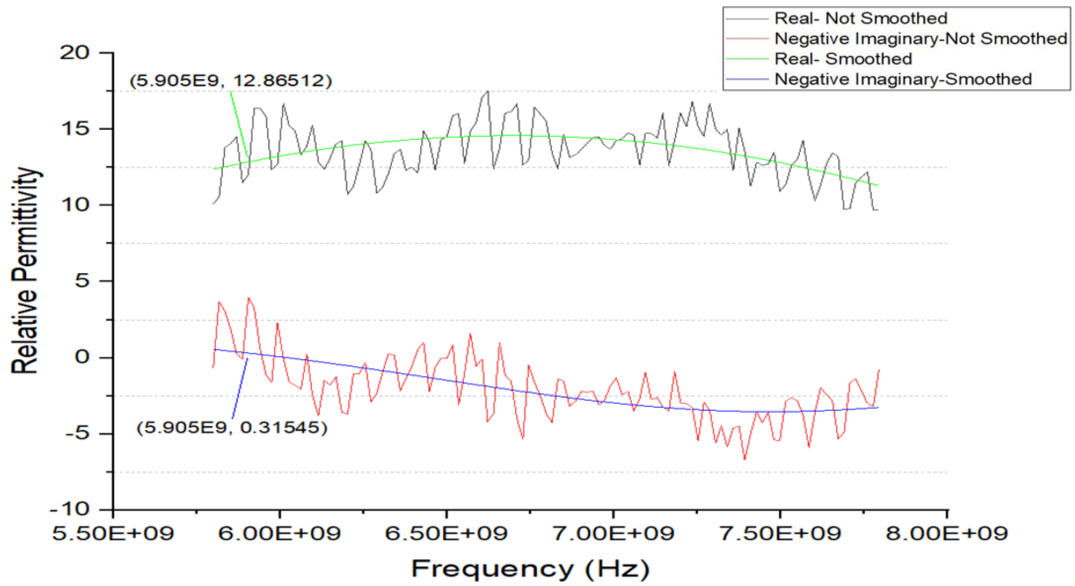

Figure 2.16: Relative permittivity of Strontium-ferrite sintered film

A synopsis of the outcomes for the ferrite films in table structure is given in table 2.4. The value in the parentheses is the average value after a Gaussian fit to all data within 5.85-7.8 GHz. The value outside the parentheses is the value at 5.9 GHz.

Table 2.4: Obtained relative permeability and relative permittivity of materials at 5.9 GHz

Materials	Relative Permeability		Relative Permittivity	
	Real Part (μ’)	(μ’’)	Real Part (ε’)	(ε’’)
Bi-Ferrite Ink (30.3um)	7.82 (8.77)	2.88 (3.55)	3.49 (4.04)	3.43 (0.75)
Bi-Ferrite Sintered (19um)	13.25 (15.05)	7.13 (-0.70)	5.74 (6.80)	6.62 (4.30)
Sr-Ferrite Ink (31.5um)	9.70 (11.4)	3.16 (3.58)	4.28 (4.90)	3.49 (0.85)
Sr-Ferrite Sintered (22.4um)	26.91 (29.51)	2.62 (1.80)	12.02 (12.87)	3.98 (0.32)

Conclusion

In summary, several ferrite material inks have been developed and evaluated the influence of different binders and solvents. DC characterization of the ferrite materials agreed with the expected behavior of the materials. The thin film of Strontium ferrite sintered sample at the frequency of 5.9 GHz, attained a relative permeability of 29.5. The permittivity at this frequency was achieved 12.02. Therefore, this high relative permeability and relative permittivity would make this film a strong candidate to demonstrate a possible pathway for future applications for designing magnetic waveguides.

3. GRAPHENE ANTENNA SIMULATION

Design modular waveguide approaches

The concept of a modular antenna has a lot of advantage since no electric feeding network is needed as the radiators are excited using the fundamental waveguide mode and the amplitudes are adjusted in a solely mechanical way. In many applications, antennas have to withstand harsh chemical environment and therefore they have to be corrosion-resistant. The reason we also use graphene is that graphene is resistant to harsh environmental factors such as rain, snow, heat, surface friction (A. Scida,2018). Graphene is a flexible, strong, lightweight, transparent and a super high conductive material (M.A. Monne, 2017). The discovery of graphene, its potential utilization is foreseen in many fields.

We tried to simulate a graphene antenna or metallic antenna for coupling the incoming radiation coming from a patch antenna to propagate radiation along the graphene antenna instead of all direction. We have found that a graphene antenna or metallic antenna is capable of coupling the incoming radiation coming from a patch antenna. In waveguide design, the graphene antennae are closed by the adjacent antenna to get higher directivity of signal along the waveguide design. We have simulated the antenna at 5.9 GHz frequency as an example of c-band application. However, this design is easily scalable to other frequencies.

Antenna geometry

A patch antenna radiating at 5.9 GHz is designed and verified using HFSS. The patch antenna is used to excite the graphene antenna. The optimized graphene antenna has a dimension of 1.54 cm $\times$ 2 cm, with substrate of 25.4 cm $\times$ 17 cm $\times$ 0.0125 cm, the distance between the center of patch antenna and the first loop antenna is 3.3 cm. Fig. 3.1

shows the design of graphene antenna. To decide the best spacing between two graphene antenna, we have put the graphene antenna in various ways from the fix patch antenna so as to accomplish better outcomes.

The length, width and positon of graphene antenna, are giving improvement in gain seen as in the depicted figure Fig. 3.1. The higher width makes strong influence on the transition effect as waveguide antenna.

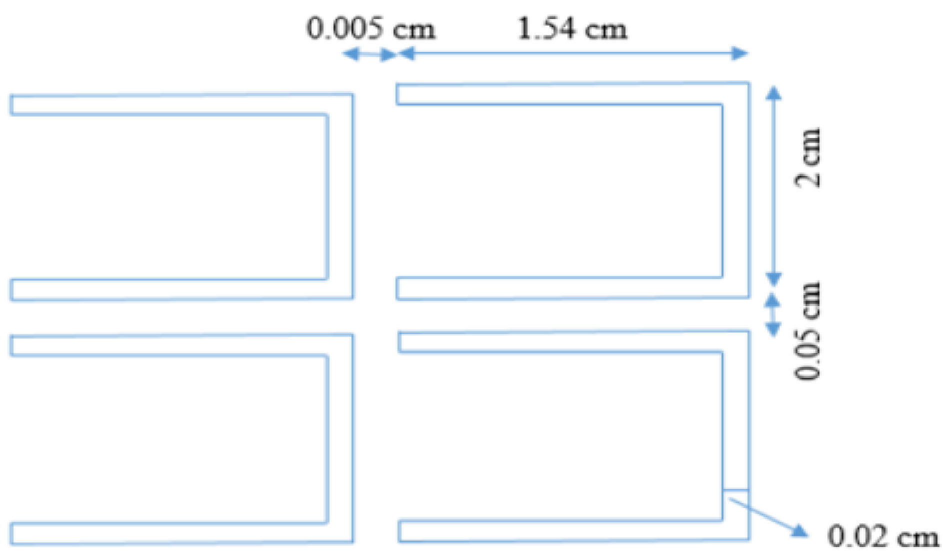

Figure 3.1: The design of graphene antenna

The distance from the one graphene antenna in the top right corner to the other graphene antenna left is 0.005 cm. The distance from the graphene antenna in the top right corner to the one below it is 0.05 cm. So, the distance of the center from the top right corner antenna to the other center of the antenna below is 2.10 cm.

Then Single, and 16*7 graphene loop antennas were added along with the patch antenna, with thickness of 55 microns, substrate thickness of 125 microns.

Kapton Substrate having relative permeability of 1 and relative permittivity of 3.5 and conductivity of 0.0193 Siemens/m was used in the simulation. The substrate of choice was Kapton due to the higher heat tolerance during thermal oven drying and photosintering. However, PET film was also an acceptable option. These photosintered films showed excellent adhesion to the substrate and could be flexed without issue.

Simulate conformal graphene antenna performance

In this experiment, a rectangular patch antenna is used to excite the graphene loop antenna in order to check the gain of overall antenna when a graphene antenna having relative permeability of 1, relative permittivity of 1.5 and conductivity of 200k is introduced near the source antenna. Return loss or S_{11} was obtained -29.2518 dB and for "phi 90 "at -81 degree angle maximum gain was obtained 8.3228 dB. S_{11} represents how much power is reflected from the antenna. We have simulated the patch antenna on H plane.

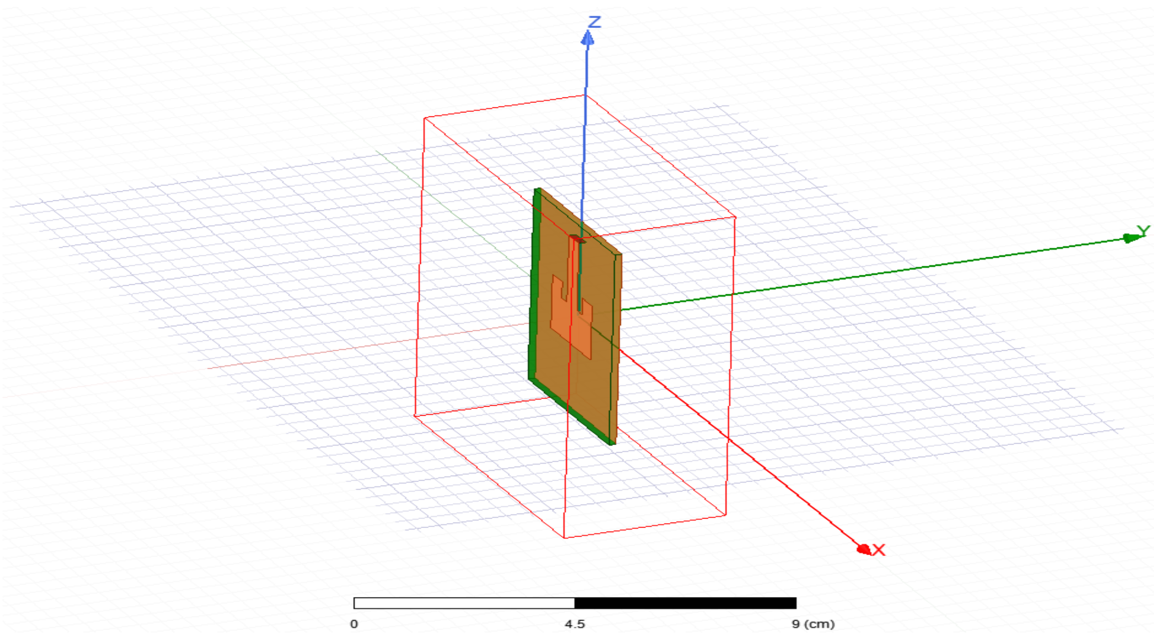

Figure 3.2: A rectangle patch antenna (as a source)

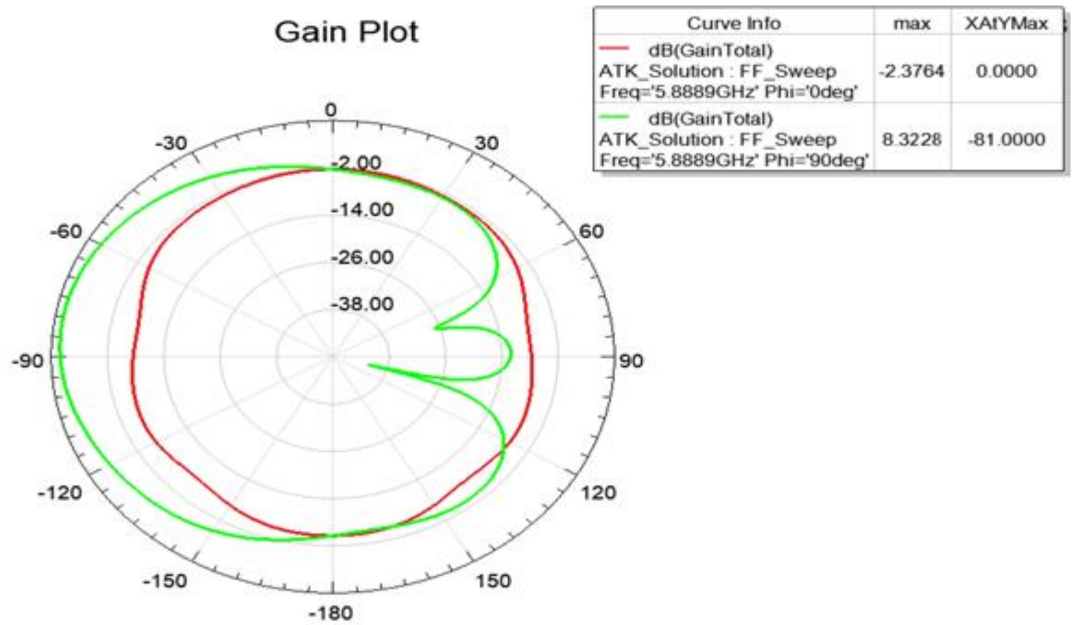

Figure 3.3: Gain of a rectangle patch antenna

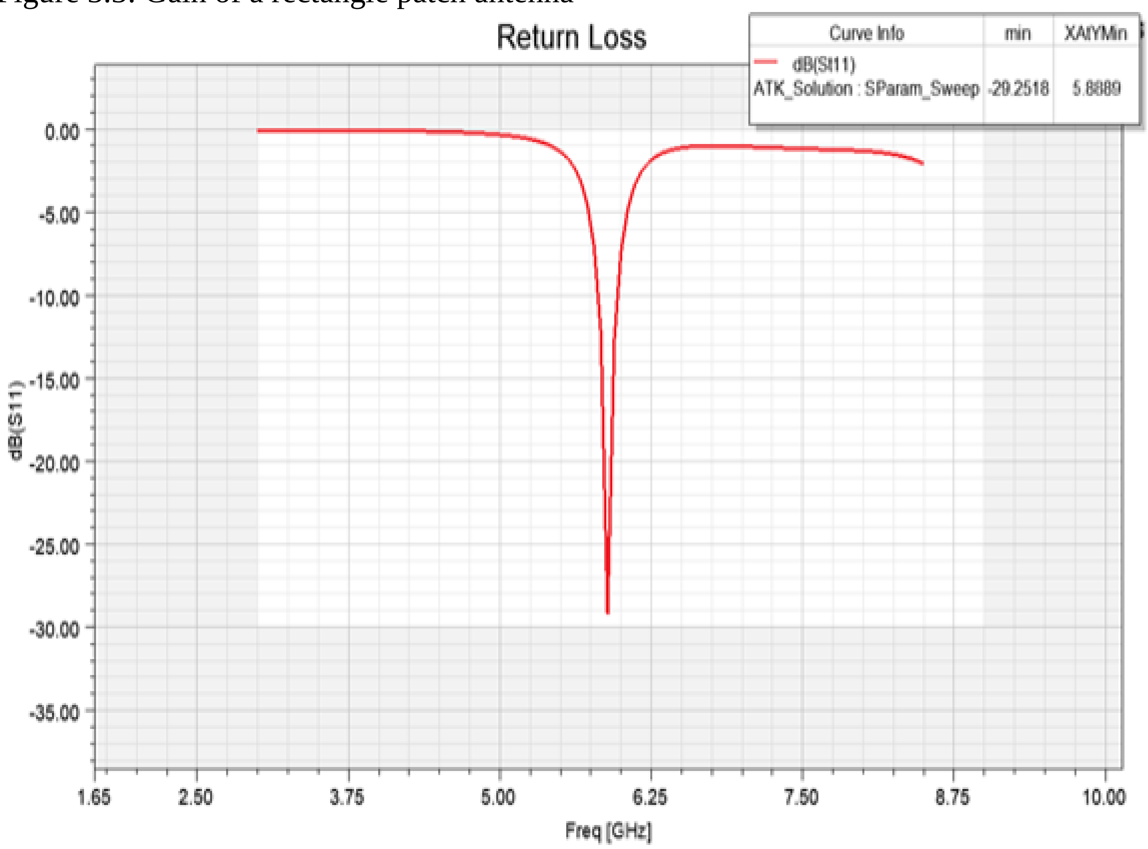

Figure 3.4: Return loss of a rectangle patch antenna

For graphene antenna simulation, we have optimized the antenna design for two distinct widths, for example, 1000 microns and 200 microns while other boundary was kept same value. Relative permeability and Relative permittivity of the proposed antenna was viewed as 1, having thickness 55 micron, and conductivity 200 k Siemens/m. The distance between the center of patch antenna and the first loop antenna is 3.3 cm. So as to see the gain change, in the simulated the graphene antenna.

Single graphene antenna

The designed single graphene antenna is placed on kapton substrate having grounding and tested by changing the position of substrate and graphene antenna to reshape the approaching radiation pattern. In the simulation, we have tried with grounding back of substrate since the graphene antennas are traditionally metallic. Single graphene antenna having 1000 microns' width simulation results are shown below.

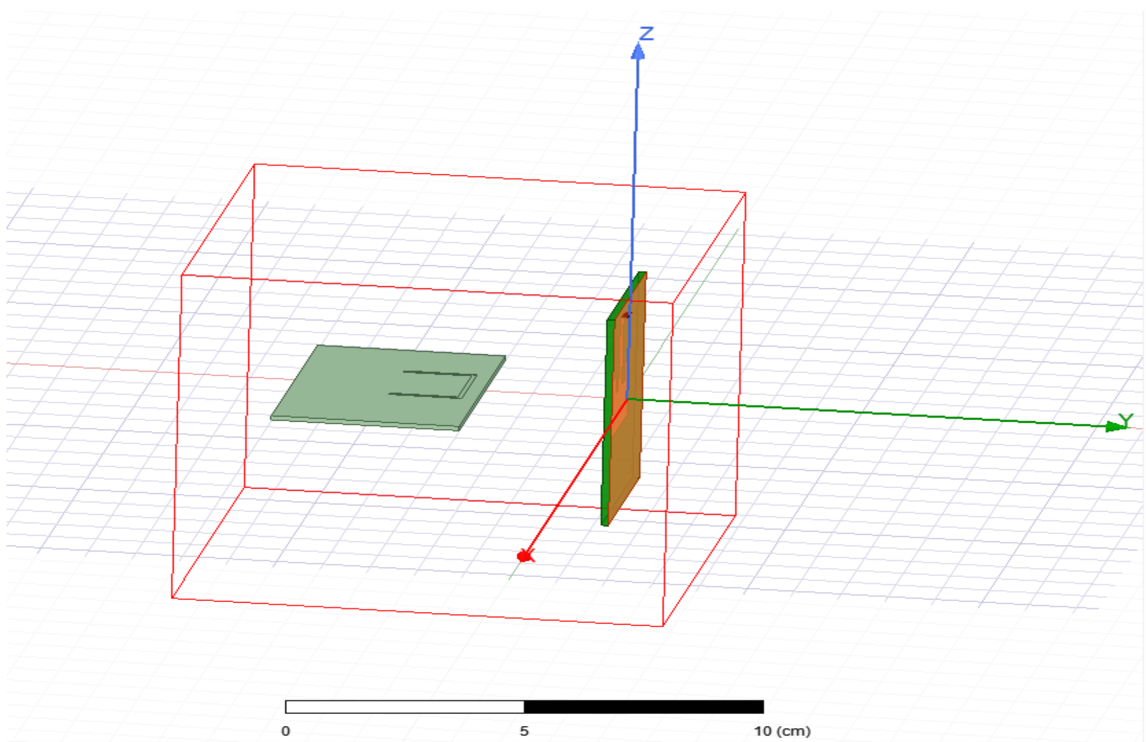

Figure 3.5: Single graphene antenna

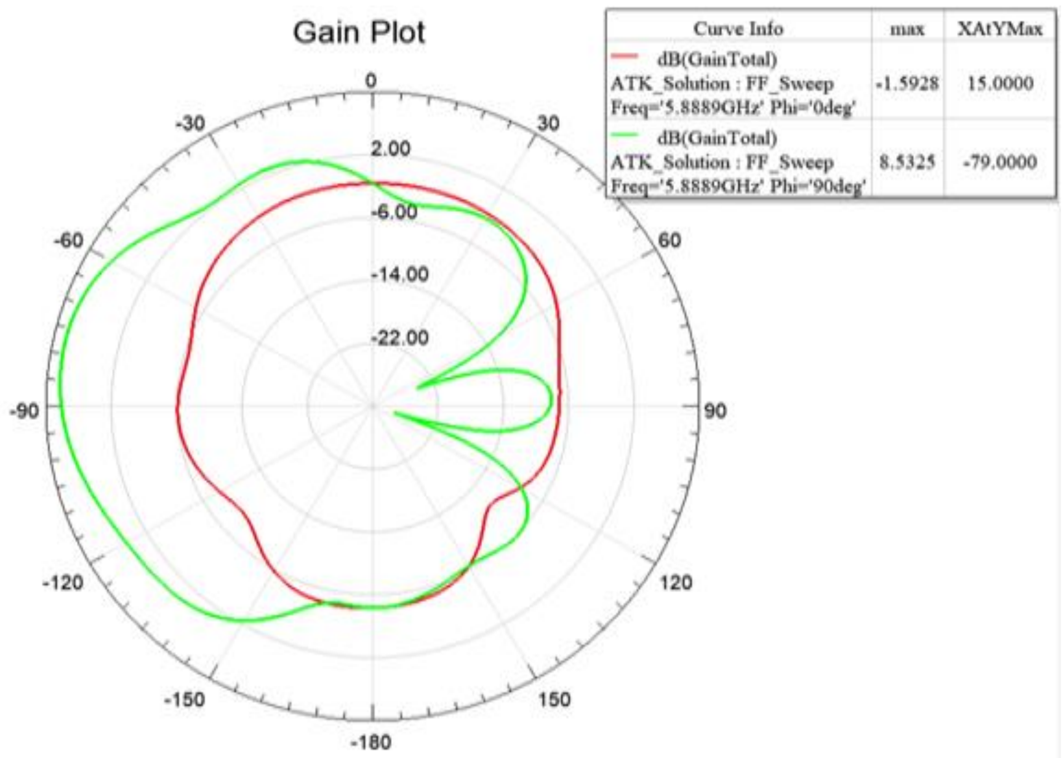

Figure 3.6: Gain of single graphene antenna.

Fig 3.6, shows that 0.2091 dB overall gain improved and we move to replace the graphene antenna with less width of 200 microns rather than 1000 micron.

Single graphene antenna having 200 microns' width simulation results are shown below. For less width of graphene antenna, Fig 3.7, additionally demonstrated that graphene antenna while grounding has better outcomes about 0.13 dB. However, the higher width makes strong impact on the transition effect as waveguide antenna contrasted with lower width of graphene antenna.

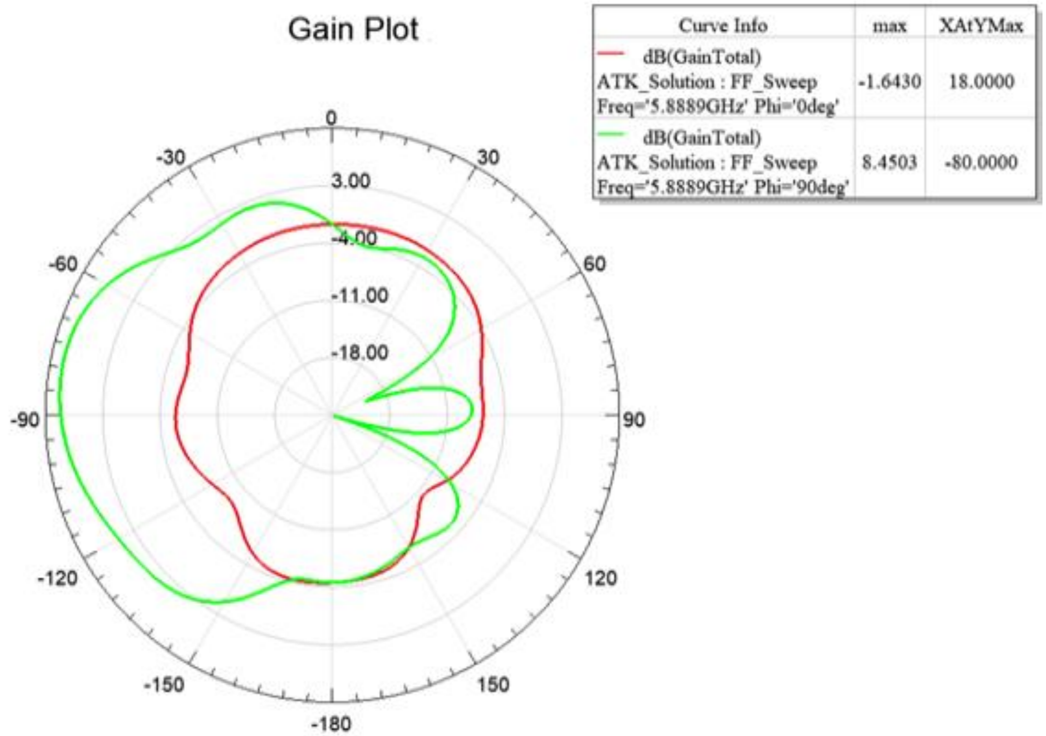

Figure 3.7: Gain of single graphene antenna having less width

16*7 graphene antenna

In Fig. 3.8, we have added the optimized graphene antenna more in a letter size paper to reshape the incoming radiation pattern. The total of 112 elements of single graphene antenna having 1000 microns' width simulation results are shown below.

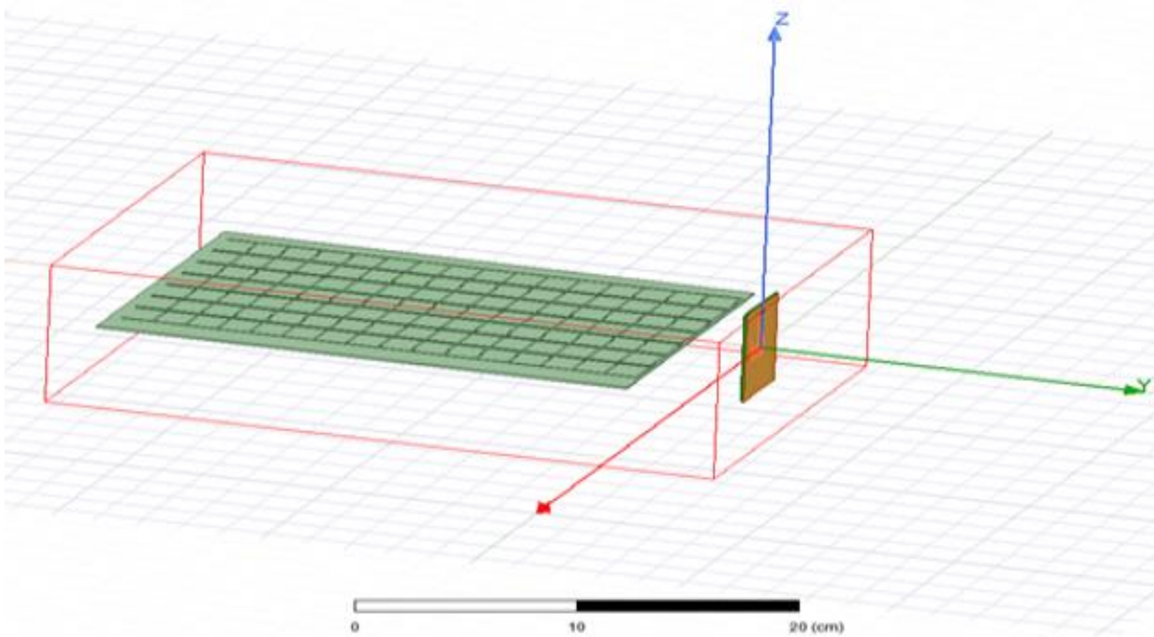

Figure 3.8: 16*7 graphene antenna

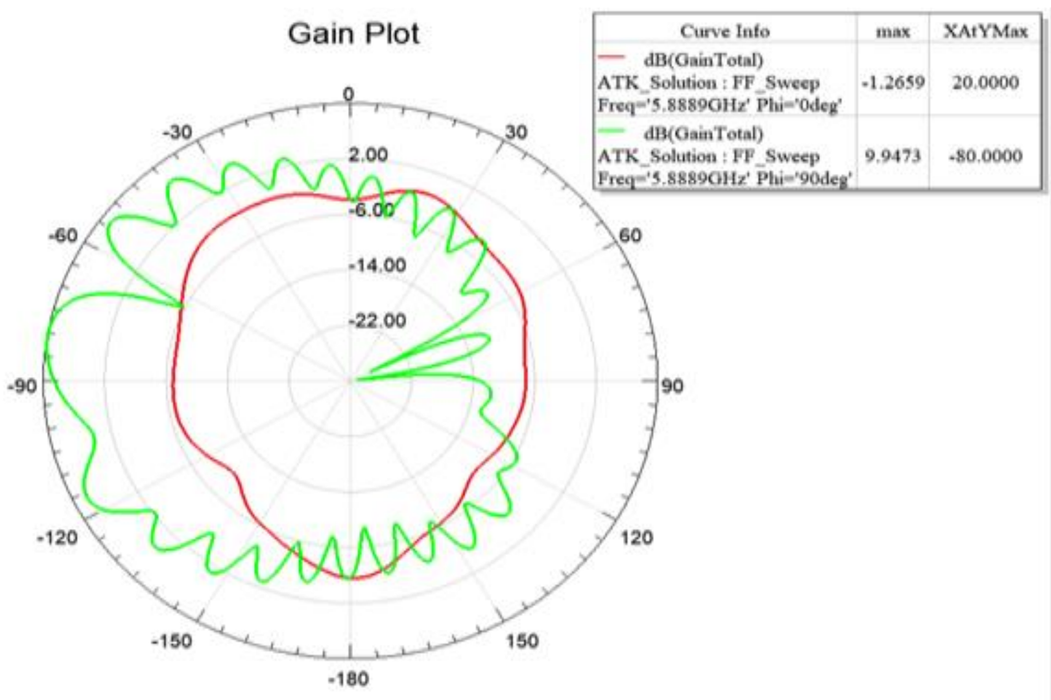

Figure 3.9: Gain of 16*7 graphene antenna

Above Fig. 3.9 shows that when we added 16*7 array graphene antenna adjacent to each other graphene antenna, overall 1.6245 dB gain is improved. An array graphene antenna is a set of multiple connected antennas which work together as a single antenna, to receive incoming radiation from patch antenna. The results show that the array of graphene antenna is demonstrated to enhance the signal of patch antenna along the magnetic/graphene antenna structure direction.

16*7 graphene antenna having 200 microns' width simulation results are shown below.

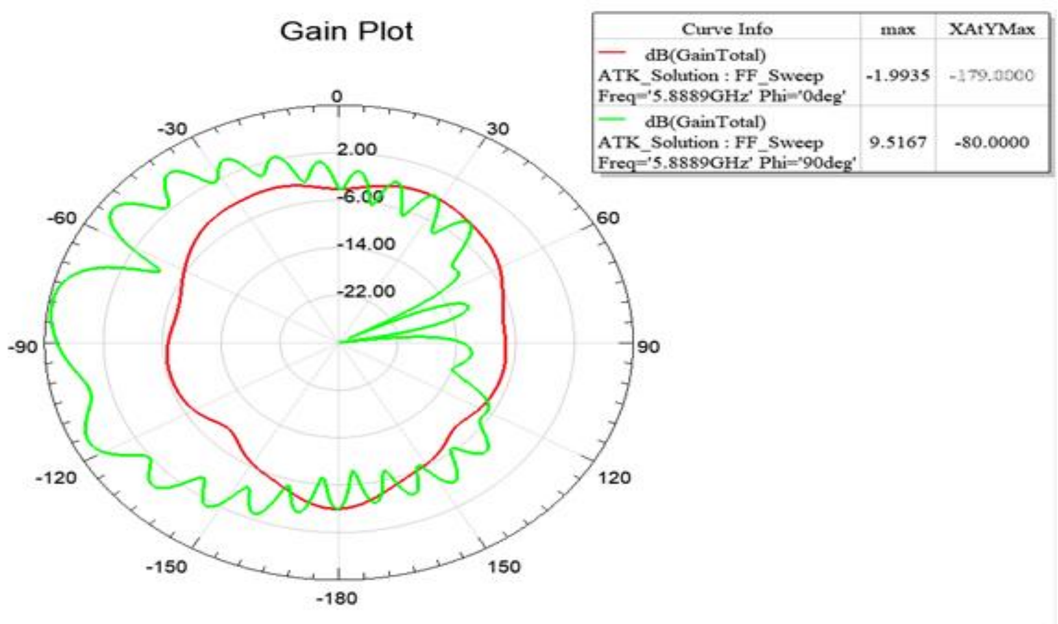

Figure 3.10: Gain of 16*7 graphene antenna having less width

Fig. 3.10 also demonstrated that if we include more loop in the designed, then it will increase the overall gain. However, the higher width graphene antenna provides more reshaped radiation contrasted with lower width of graphene antenna

Graphene antenna fabrication

AutoCad 2018 version was used to draw the schematic of the single patch antenna. After successfully printing the antenna with Dimatix inkjet printer, the far field patterns were measured. A Vector network analyzer is used in order to normally intended to measure the behavior of electrical networks. it consists of two ports one input and one output port, two Standard horn antennas covering 5.9 GHz have used in order to transmit/receive the desire signal to the printed antenna for the measurement.

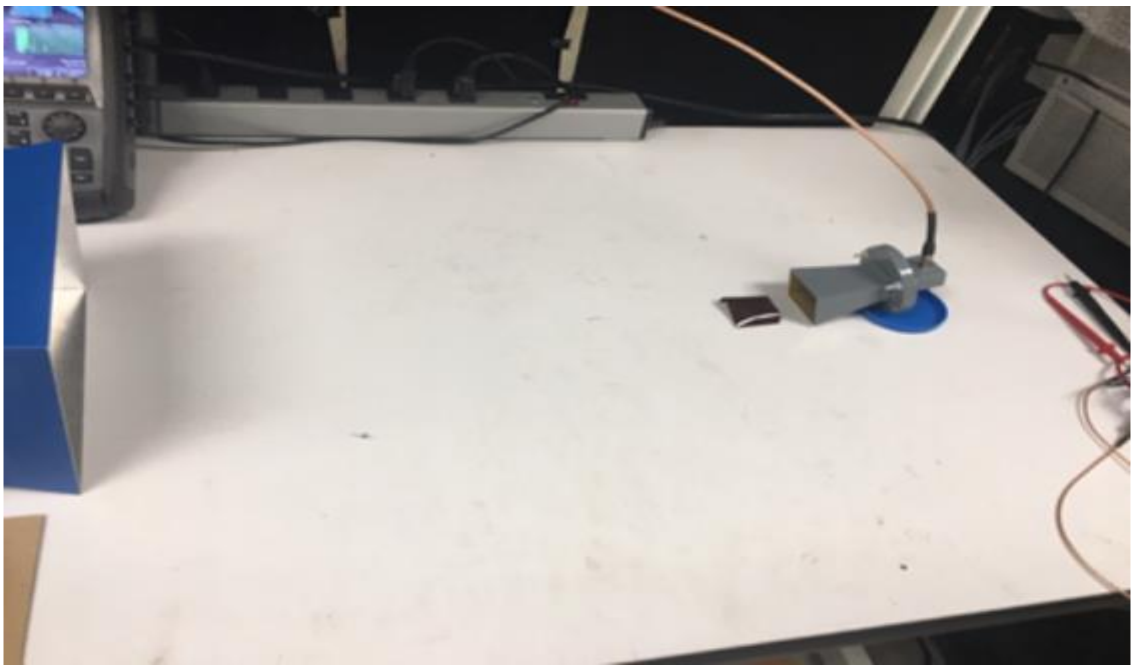

Figure 3.11: Test setup for gain measurement

We have placed two horn antenna 24 inch apart from one to another. We tried 3 placements:

1) an inch from the left antenna,

2) an inch from the right antenna, and

3) in the middle.

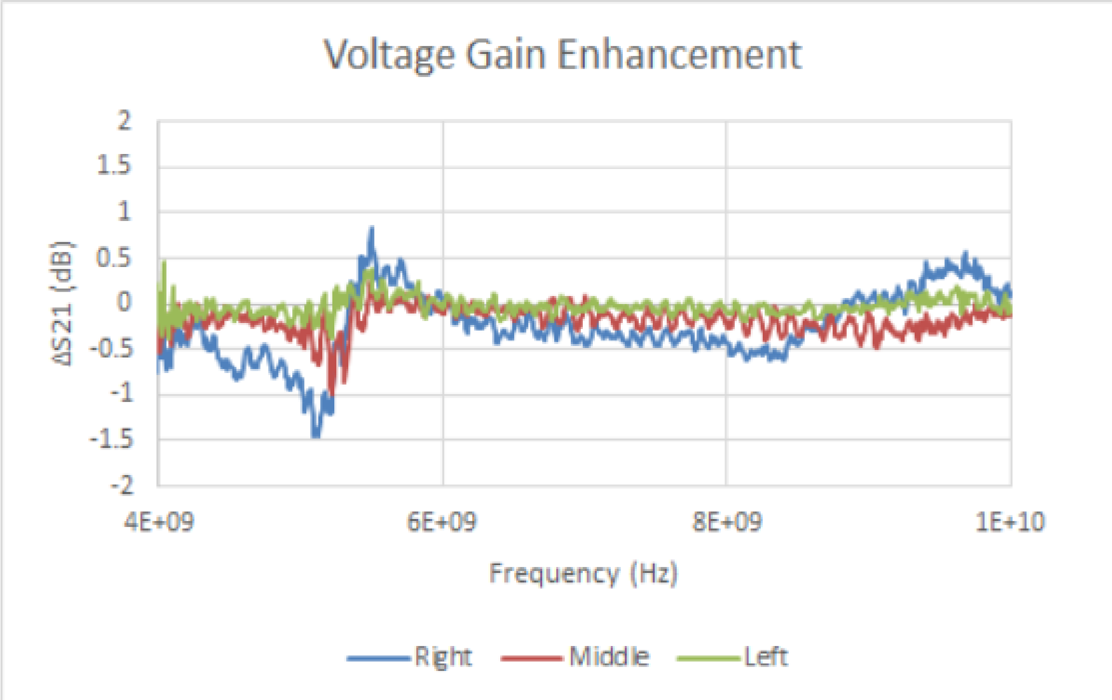

Figure 3.12: Voltage gain enhancement of single graphene antenna

There is ~0.15 dB enhancement for the placement in the attached picture where it was an inch from the right horn. The enhancement of ~0.15 dB is similar as simulated value.

Conclusion

A modular graphene waveguide antenna is introduced and tried in this work. This single graphene antenna will likewise fill in as the establishment of the work on graphene array antenna. Moreover, a remarkable procedure of creating single graphene antennas with conductive graphene-based material and inkjet printing technique was introduced. Fabricated single graphene antenna using inkjet printing technique has a reasonable agreement between simulated value and measured value. The printed single loop graphene antenna indicated a superior increase of 0.15 dB.

4. FERRITE ANTENNA SIMULATION

Antenna geometry

After successful design of single graphene antenna as well as array of graphene antenna, we move to our fundamental goal for this proposal, which is design of magnetic peel and stick ferrite antenna. From the characterization results, we have found the best relative permeability 29 and relative permittivity 12 for the strontium ferrite which used for the proposed antenna so as to show how the ferrite antenna changes the far field radiation pattern of the patch antenna. The conductivity of the ferrite antenna loop was measured to be 4 Siemens/m.

However, the ferrite antenna has also a dimension of 1.54 cm $\times$2 cm, with substrate of 25.4 cm $\times$17 cm $\times$0.0125 cm, the distance between the center of patch antenna and the first ferrite loop antenna is 3.3 cm were kept same as the graphene antenna. We used same distance between patch with first ferrite antenna loop in order to compare data to find out the effect of the simulation results.

Then single, 2*2 and 16*7 ferrite loop antennas were added along with the patch antenna, with thickness of 55 microns, substrate thickness of 125 microns, we have used Kapton Substrate having relative permeability of 1 and relative permittivity of 3.5 in the simulation.

Simulate conformal magnetic waveguide performance

For ferrite antenna simulation, we have used the antenna design for widths of 200 microns. In HFSS simulation, we applied Perfect H to ferrite magnetic antenna since ferrite materials are magnetic. Perfect H is a perfect magnetic boundary. It causes the magnetic field (H-field) to be in a direction normal to the surface that it is assigned to.

The perfect H boundary forces the tangential component of the H-field to be the same on both sides of the boundary. For internal planes, this results in a natural boundary through which the field propagates. For planes on the outer surface of the model, this results in a boundary that simulates a perfect magnetic conductor (the tangential component of the H field is zero).

Electromagnetic waves are made up of Electric field often called the E-field and magnetic fields known as H-fields. The H-field is a vector quantity (has a magnitude and direction) and is measured in amps per meter. The H-field is orthogonal to the direction of propagation in a plane wave, as well as perpendicular to the E-field. It is the interaction of the E-field with the H-field in space that allows for wave propagation. For ferrite antenna, exciting an oscillating H-field in the antenna with incoming radiation would be able to, in turn, excite the E-field. Therefore, it will propagate the signal along the ferrite antenna.

Single ferrite antenna

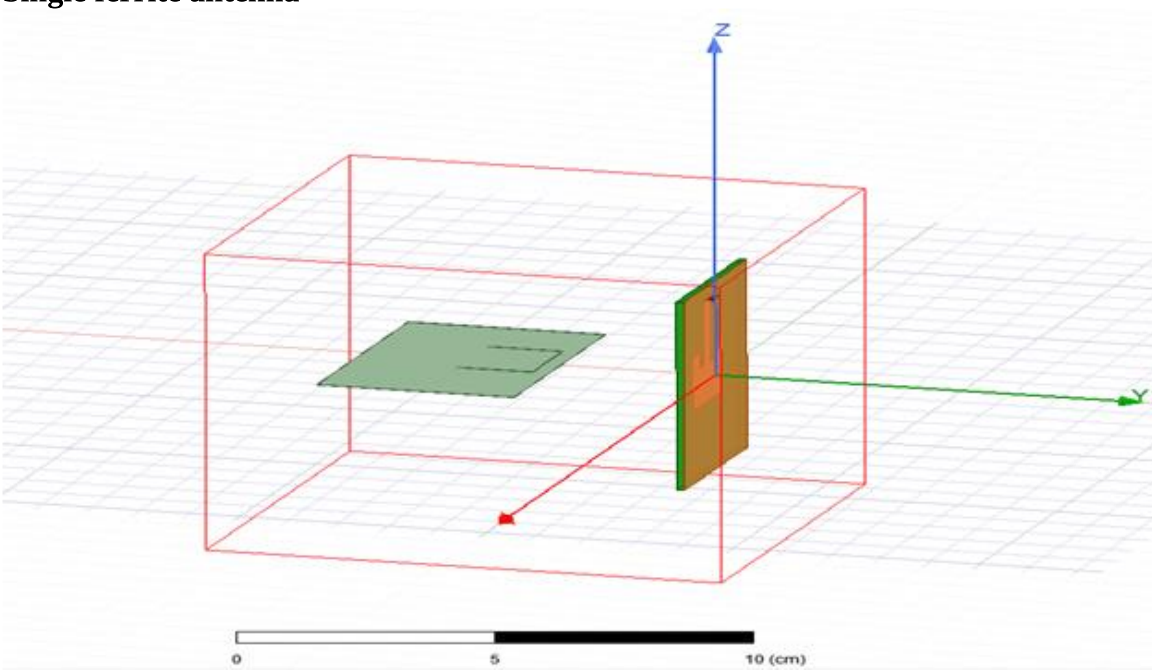

Figure 4.1: Single ferrite antenna

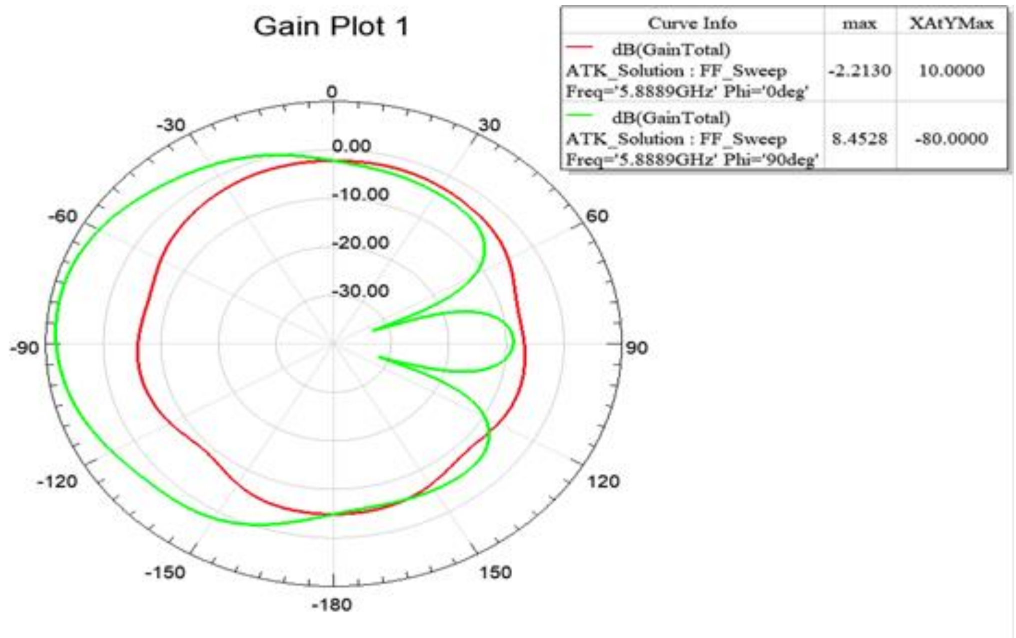

Figure 4.2: Gain of single ferrite antenna

From the above Fig. 4.2, it can be seen that good amount power received from the patch antenna by the single loop ferrite antenna. The measure of power got by the single circle ferrite is almost 0.13 dB, this is exceptionally good and fills in as a proof that the ferrite antenna is appropriately structured. The S11, also called the reflection coefficient, guarantees that a very minimal amount of energy, at least around 5.9 GHz, is actually reflected back to the input performing very well.

2*2 ferrite antenna

In this 2*2 array simulation, we have used four ferrite loop to enhance the total gain. From the Fig. 4.4, it can be seen that the 2*2 ferrite array antenna enhanced the gain almost 0.20 dB.

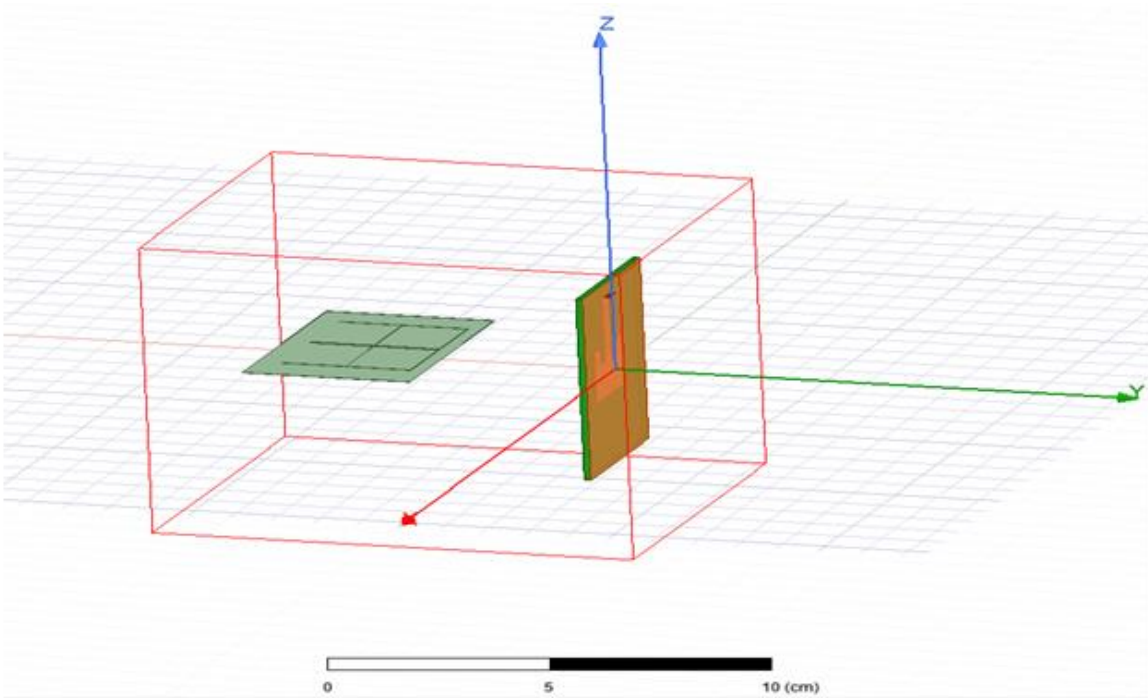

Figure 4.3: 2*2 ferrite antenna

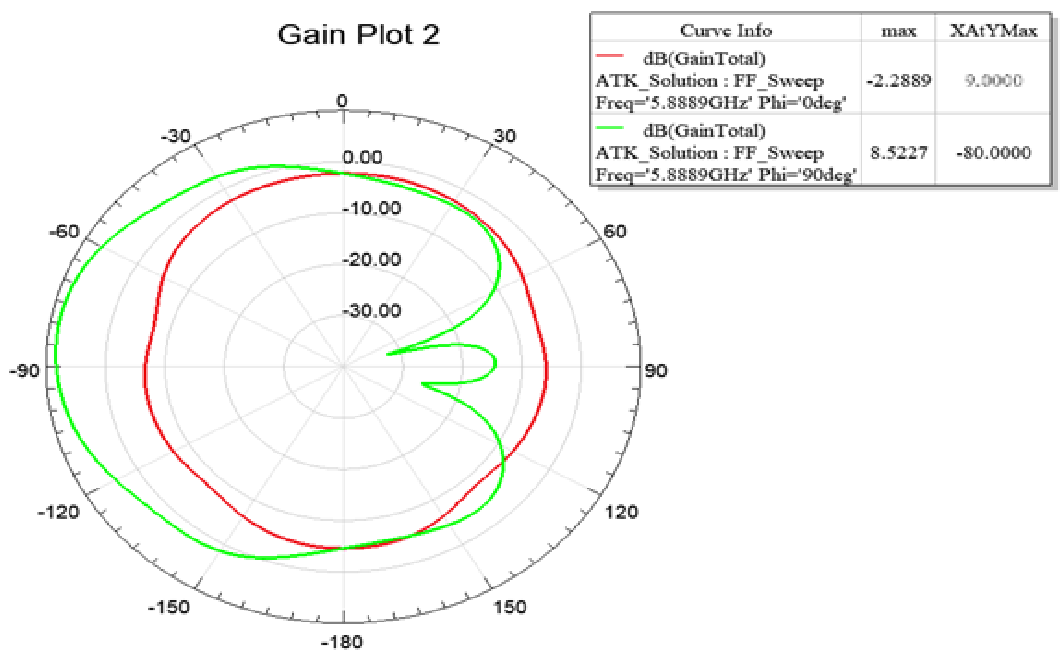

Figure 4.4: Gain of 2*2 ferrite antenna

16*7 ferrite antenna

For 16*7 array simulation, we have included total of 112 components of ferrite loop to improve maximum overall gain.

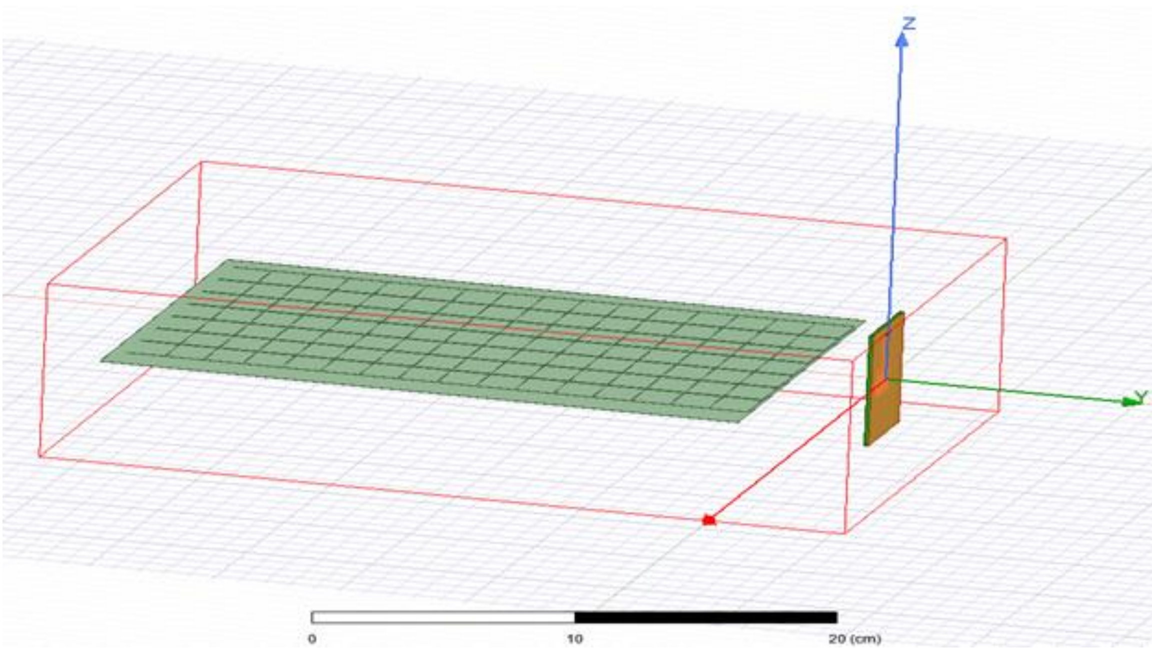

Figure 4.5: 16*7 ferrite antenna

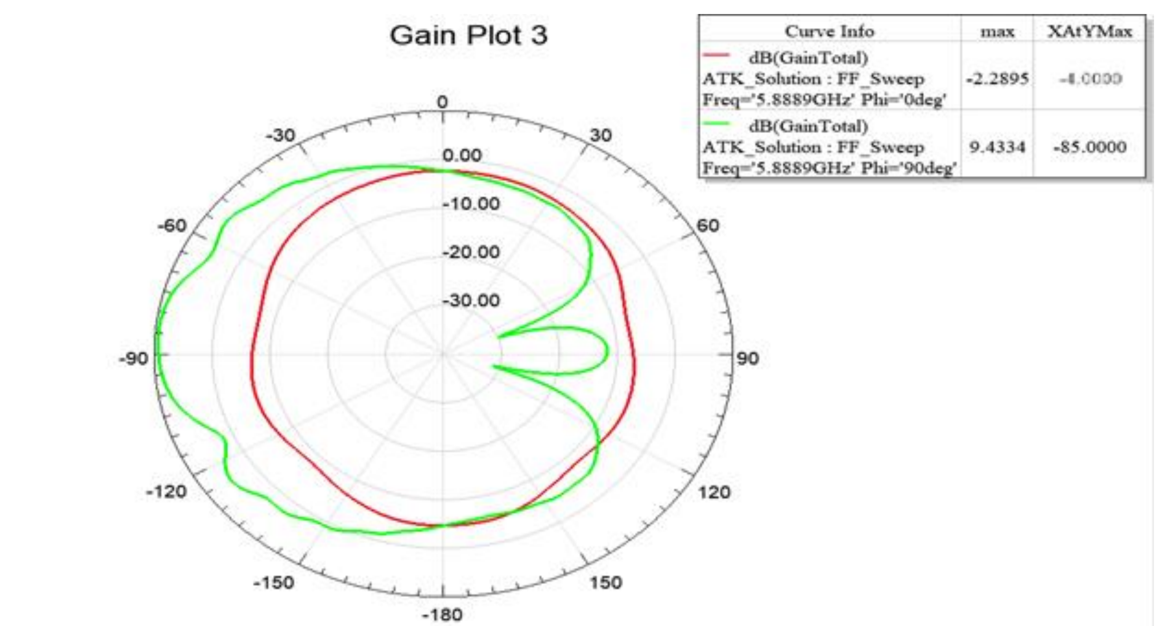

Figure 4.6: 16*7 Gain of ferrite antenna

As more elements added to the simulation and optimization carried out as to see more amount of gain. From the above figure we can see that the enhancement of power got by the 16*7 ferrite array antenna with less than a letter paper size is almost 1.11 dB, which is a significant amount gain obtained from the simulation.

However, one challenge for this modular design is that it relies on films with high permeability at 5.9 GHz.

Conclusion

Comparing the Single ferrite loop and array of ferrite loop gain patterns, it is found that 0.13 dB gain was achieved by single loop whereas 1.11 dB gain increase was achieved by adding 16 by 7 loop antennas. We have added more elements to the simulation and optimization carried out. This result establishes the capability of a magnetic/graphene antenna to enhance the radiation coming from the patch antenna.

5. CONCLUSION AND FUTURE WORK

Conclusion

In this thesis, at first we verified the rectangular microstrip patch antenna using HFSS that can support 5.9 GHz was used as a source of radiation. The physical dimensions of the designed antenna were then tuned and the effect of tuning the dimensions on several antenna parameters like bandwidth and gain were observed. Then, we performed a preliminary modeling investigation of a modular waveguide.

We have used conductive graphene and ferrite material in the models of modular designs in order to increase performance and design options. The designed Single graphene antenna was placed on kapton substrate to investigate its effect on gain. After that, the designed antenna is used to create an array antenna with more elements. The purpose of implementing the array of the initially designed graphene loop was to study the enhancement of antenna parameter gain and bandwidth with respect to the antenna parameters of the single element itself.

We intend to increase the opportunity for a successful design. The relevant material parameters were determined using DC and high frequency analysis. Models of waveguides were performed based on these parameters to evaluate performance.

After successful design of the graphene antenna, we have tested for the ferrite antenna. However, the designed ferrite antenna shows higher gain than graphene antenna with similar feature sizes.

Future work

In the future, we could accomplish more work on building up the ferrite material to have higher permeability. The substrate of decision for the greater part of the was utilized Kapton because of the higher heat tolerance during thermal oven drying and photosintering. In any case, PET film could be additionally a worthy alternative. These photosintered films likewise has great grip to the substrate and could be flexed without issue. Finally, if time allows, we could print the ferrite antenna and evaluate its performance.

REFERENCES

Rumsey, V.; Weeks, W. Electrically small, ferrite-loaded loop antennas. *1958 IRE International Convention Record* **1958**, 165.

Auckland, D.; Daniel, C.; Diaz, R. A New Type of Conformal Antenna Using Magnetic Flux Channels. **2014**, 372-375.

Simpson, T. L. Designing an electrically small ferrite-loaded loop antenna for optimum performance. *Antennas and Propagation Society International Symposium* **2007**, 5427.

McLean, J.; Sutton, R. An efficient, low-profile antenna employing lossy magneto-dielectric materials. *2012 IEEE International Workshop on Antenna Technology (iWAT)* **2012**, 261.

Wan, S.; Tang, J.; Wolff, R. S. In *Tilte*2008; IEEE.

Rosales, M.; Montiel, H.; Valenzuela, R. Magnetic permeability and relaxation frequency in high frequency magnetic materials. *Materials Research Society Symposium Proceedings* **2001**, *674*, U1.8.1.

Sebastian, T..Megneio Dielectric Wire Antennas Theory and Design

Kraftmakher, Y. Eddy currents: Contactless measurement of electrical resistivity. *American Journal of Physics* **1999**, *68*, 375-379.

J. Chen, G.S., S. Hunter, V. S. Babu, M. S. Seehra, *Observation of superparamagnetism in rf-sputtered films of zinc ferrite.* J. Magn. Magn. Mater, 1995. **vol. 146**: p. 291-297.

Chao, L., Sharma, A., Afsar, M. N., Obi, O., Zhou, Z., & Sun, N., *Permittivity and permeability measurement of spin-spray deposited Ni-Zn-ferrite thin film sample.* IEEE Transactions on magnetics, 2012. **48(11)**: p. 4085-4088.

Chen, L.F. Ong, C.K. Neo, C.P. Varadan, V.V. and Varadan, V.K. *Microwave Electronics Measurement and Materials Characterization, 2004.*

Youngs, I., et al., *Dielectric relaxation in metal-coated particles: the dramatic role of nano-scale coatings.* Journal of Physics D: Applied Physics, 2005. **38**(2): p. 188.

Bahadoor, A., Y. Wang, and M.N. Afsar, *Complex permittivity and permeability of barium and strontium ferrite powders in X, KU, and K-band frequency ranges.* Journal of applied physics, 2005. **97**(10): p. 10F105.

Mathew, D.S. and R.-S. Juang, *An overview of the structure and magnetism of spinel ferrite nanoparticles and their synthesis in microemulsions.* Chemical engineering journal, 2007. **129**(1-3): p. 51-65.

M. A. Monne, E. Enuka, Z. Wang, and M. Y. Chen, “Inkjet printed graphene-based field-effect transistors on flexible substrate,” *Proc. SPIE 10349, Low-Dimensional Materials and Devices*, 1034905 (2017).

Sebastian, T.; Clavijo, S.; Diaz, R.; Daniel, C.; Auckland, D. A new realization of an efficient broadband conformal magnetic current dipole antenna. *Antennas and Propagation Society International Symposium* **2013**, 1290.

Scida, S. Hauqe. Application of graphene-based flexible antennas in consumer electronic device, Material today 2018, 21

Katsuhiko Inaba, High Resolution X-Ray Diffraction Analyses of (La,Sr)MnO3/ZnO/Sapphire(0001) Double Heteroepitaxial Films, Advancesin Materials Physicsand Chemistry, 2013, 3, 72-89

Alexandre, Vicente, The Step by Step Development of NRW Method, IEEE. 2011